Addis Ababa University
Addis Ababa Institute of Technology
School of Electrical and Computer Engineering

STUDY AND ANALYSIS OF GEOMAGNETIC INDUCED CURRENT IN ETHIOPIAN ELECTRIC POWER SYSTEM

By: Habib Abdurahman

A Thesis Submitted to the School of Graduate Studies in Partial Fulfillment of the Requirement of Master of Science in Electrical Power Engineering

July, 2021
Addis Ababa, Ethiopia

Study and Analysis of Geomagnetic Induced Current in Ethiopian Electric Power System.

By

Habib Abdurahman

MSc Thesis

Submitted in Partial Fulfillment of the Requirement for Masters of Science in Electrical Power Engineering

Addis Ababa Institute of Technology

School of Electrical and Computer Engineering

Signature

1. **Dean, School of Electrical and Computer Engineering**

   Dr. Bisrat Derebssa _____

2. **Advisor**

   Dr. Mengesha Mamo _____

3. **Internal Examiner**

   Prof. Nagendra Singh _____

4. **External Examiner**

   Dr.-Ing Getachew Biru _____

Declaration

I, the undersigned, declare that this MSc thesis research is my original work, has not been submitted in part or in whole, at any other university and all sources, and materials used for the thesis work, and the organizations and individuals who contributed a lot during the development of this study have been acknowledged.

My research was conducted at Addis Ababa Institute of Technology under the supervision of Dr. Mengesha Mamo.

Submitted by:

…….

Habib Abdurahman

ID No. GSR/2200/10

Acknowledgment

First of all, I would like to give my warm thanks to the Almighty Allah, who gave me patience and blessing to conduct this master research thesis.

Secondly, I would like to give my thanks to my advisor Dr. Mengesha Mamo. His continuous feed back to my research is valuable to me.

Thirdly, I would like to express my sincere thanks to Dr. Tilaye Tadesse Asfaw who is a research engineer in NASA Johnson space center. He gladly accepted to support and providing solar physics papers for literature reviewing and its application in electrical power system. His guidance was starting from the inception of the idea and He kindly pushed me to do interdisciplinary research. and his devotion to patiently guide me throughout the on-going stages of the research is really highly appreciated.

Lastly, I would like to give my thanks to the staffs of Ethiopian Electric Power Corporation, Addis Ababa university geomagnetic observatory and physics faculty staff, especially for feeding me the required information related to my study.

Abstract

In this master thesis the effect of GIC on Ethiopian electric power system is investigated using the power world simulator software and python coding.

GIC flowing in the transformers core lead to a higher magnetizing peak current, which produce a higher flux, that also contains a lot of harmonics. This leads to a large increase of eddy and circulating current in both windings and structural parts of the transformers, causing unnecessary heat generation. Such unnecessary heat generation causes tripping of transformers components like relays, SVC, capacitor bank controllers and burning of transformer sheet cores. GIC not only affect transformers but also affect transmission lines. The effect of GIC on power transmission lines is a high voltage drops at the receiving end due to the varied geo-magnetic and geo-electric field value.

The equatorial electro-jet magnetic field (GIC Max-H and GIC Max-L) undergoes variability in the high latitude region of Ethiopia and low latitude region of Ethiopia. The equatorial electro-jet magnetic field value for high latitude region of Ethiopia is 192 nT and the equatorial electro-jet magnetic field value for low latitude region of Ethiopia is 100 nT. The GIC is propagated from 45 degree to 315 degree eastward in the high latitude region of Ethiopia and from 135 degree to 225 degree westward in the low latitude region of Ethiopia. It is also found that the percentage of GIC flowing in the transformers core is approximately 1000 percent greater than the rated peak magnetizing current of the transformers. And finally, a GIC value of 34kA is measured in the high latitude region of ethiopia. For this GIC value of 34kA, an 80 MVAR of reactive power is absorbed by a transformers located in high latitude region of Ethiopia.

The result showed that the Impact of GIC on transformers and transmission lines is severe in High latitude region of Ethiopia compared to the low latitude region of Ethiopia. The reactive power consumptions of transformers located in high latitude region of Ethiopia is high compared to low latitude region of Ethiopia. One of the primary reasons for such difference in reactive power consumption is that, the differences in the geomagnetic fields of the two region which is 360 T in high latitude region compared to 150 T for low latitude region. Therefore, it is recommended that EEP should re-arrange the position of the transmission lines and transformers with respect to GIC propagation to minimize the effect caused by GIC.

Abbreviations and Nomenclatures

ATC	Area Transfer Controller
AMBER	African Meridian B field Education and Research.
CIM	Complex Image Method
CME	Coronal Mass Ejection
DST	Disturbance Storm Time
EEPCO	Ethiopian Electric Power Corporation
EEU	Ethiopian Electric Utility
GIC	Geomagnetic Induced Current
GMD	Geo-Magnetic Disturbance
GIC Max-H	Geo-Magnetic Induced Current extream High value
GIC Max-L	Geo-Magnetic Induced Current extream Low value
GMS	Geo-Magnetic Storm
LASCO	Large Angle Spectrometric Coronal graph instrument
MVAR	Mega Volt Amper Reactive
LP	Lehtinen-Pirjola
PCC	Point of Common Coupling
SCOPF	Security-Constrained Optimal Power Flow
SOHO	Sun and Heliospheric Observatory
SVC	Static Var Compensator

Table of Contents

List of Figures

Chapter 1

Introduction

1.1. Background

A large stream of solar particles leaves the sun continuously and creates a phenomenon called solar wind or solar storm. Occasionally the sun emits not only a constant solar wind, but also huge amount of plasma. Such emission of solar particle from the sun is known as a coronal mass ejection (CME) [1]. The process is meticulously observed by the Solar and Hemispheric Observatory (SOHO), a spacecraft launched in 1995 and located in between low Earth orbit and the sun. Figure 1-1 shows a Coronal Mass Ejection pictured by Large Angle and Spectrometric Coronagraph instrument (LASCO) on board on SOHO. Usually a CME leave the sun in the direction of Earth magnetosphere, as shown in Figure 1-1.

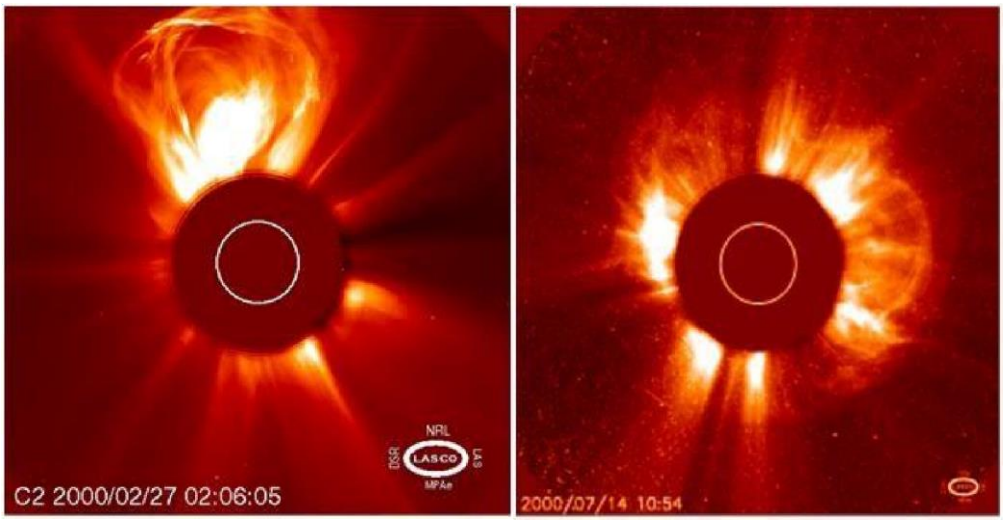

Figure 1-1 SOHO image of CME [2]

A CME contains between 1 and 10 billion tons of plasma material inside the core of the sun. It travels from the sun to earth in about 3 days. And when it arrives, it is always seen as the Aurora Borealis in the northern hemisphere or simply we called it the northern light. A CME is interacting

with Earth's magnetic field and can highly push earth magnetic field toward the earth atmosphere and moving the magnetopause and releasing current into the upper and lower atmosphere [2-3]. Now the magnetosphere and the magnetic field of the solar wind are connected and holes are created at the North Pole and the South Pole passing the charged particles from the solar wind to enter the magnetosphere. When the solar wind leaves the sun photosphere boundary, then it increase its speed until it reaches the magnetosphere of the lower earth atmosphere and due to Len'z law the interaction of the solar particles and plasma with the earth magnetic field causes a current to flow in the ionosphere boundary. This current is known as an electro jet and can reach several millions of Amperes when it reached on lower and higher atmosphere [4].

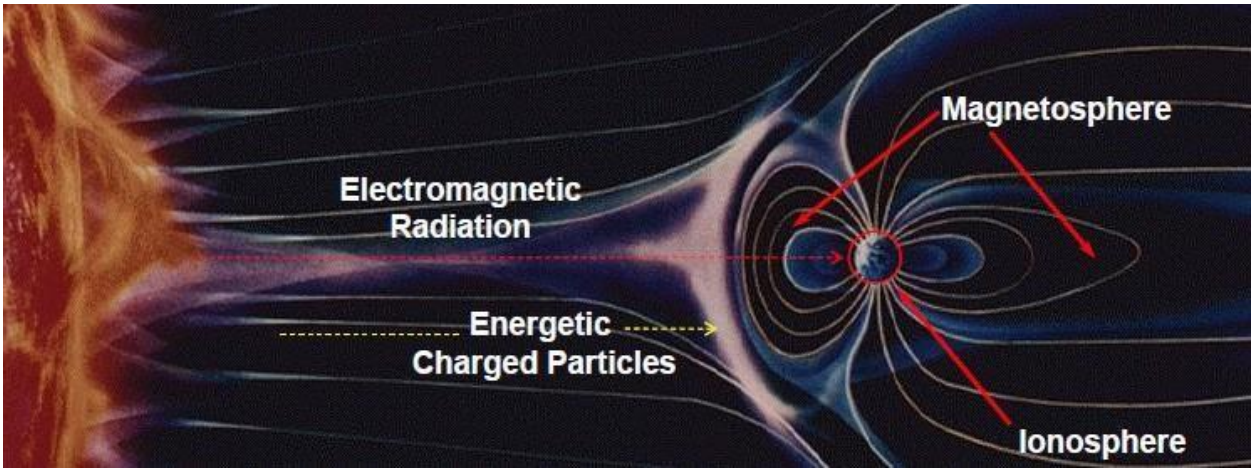

Figure 1-2 The interaction between solar electromagnetic radiation and earth magnetosphere [2]

Effects of Coronal mass ejection and solar flares on electrical power systems were observed in 1978, 1981, 1985, 1988, 1991, 1993, 1998, 2000, 2001, 2003, and 2005. Large-scale blackouts happen frequently on polar regions and caused higher risk. Severe and dangerous coronal mass ejection and solar falres events occurred in 1858, 1922, and 1988 when U.S. and Germany utilities lost electrical power transmission capability over large period of time. During the 1987 event, Canada and Germany suffered a complete blackout over long period of time and resulting in a loss of electric power for approximately 6 million peoples [4-5].

On the earth surface , the changing magnetic field and the changing electric field manifests itself as a slowly moving electric current that is produced into an electrical power conductor. Electrical

power transmission lines are invulnerable to this effect if they form a closed loop with the ground surface, which is often fairly a good conductor. This invulnerability is manifested especially in long transmission lines that happen to be oriented appropriately with respect to the changing magnetic field and electric field [5]. This effect is generally termed as geomagnetically induced current (GIC). Because the magnetic field and the electric field and changes slowly, the induced current is quasi-static direct current (DC). The area of the single-turn loop is determined by the electrical power line and a ground return is very high , the current induced is also quite large [6].

1.2. Problem Statement

Geomagnetic storms have a potential to change the Earth's magnetic field and induce electric currents in the regions of both magnetosphere and ionosphere of the earth. When a sufficient geo-voltage is created by the plasma of CME and solar flares in the magnetosphere and ionosphere region of the upper atmosphere, then a high amount of Geomagnetic Induced Current or GIC is starting to flow in the electrical power transmission line and transformer through its neutral connection.

In this study the effect of GIC on transformers and Transmission lines of Ethiopian electric power system has been investigated and possible mitigation technique has been recommended.

1.3. Objectives

The general objective of this thesis is to study the solar storm and analyze the effects of GIC on Ethiopian electric power system element.

The specific objectives of this thesis are as follows:

- ✓ To analyze the root cause of the GIC in Ethiopian Electric Power system
- ✓ To study and analyze overloading of power transformers from the severity consequence of GIC
- ✓ To study and analyze the effect of GIC in transmission lines.
- ✓ To study and analyze the reactive power loss in transformers caused by GIC
- ✓ To study the effect of GIC on transformers peak magnetizing current.
- ✓ To study the propagation of GIC in transmission lines and transformers.

1.4. Literature Review

As seen from Figure 1-3 below, the consequences from GICs on transformers are many which the transformer may be a crucial component with reference to understand how the facility system respond There are other components within the power system that area suffering from GICs, e.g. generators, high voltage synchronous motors and protection relays, but an in depth description of the GIC effects of those is beyond the scope of this master thesis research.

Nonetheless, due to the relationship between the various components in power system**,** it's vital to research the GIC response of all critical components to be ready to understand and well predict the results of GICs [7]. To solar storms and the way to mitigate the GIC effects. Still, an important description of possible relay protection failure under the influence of GICs are going to be given thanks to its importance: Poorly adjusted protection schemes may cause false trips which may cause cascading failures and black out. this is often what happened under the Hydro-Québec event [8]

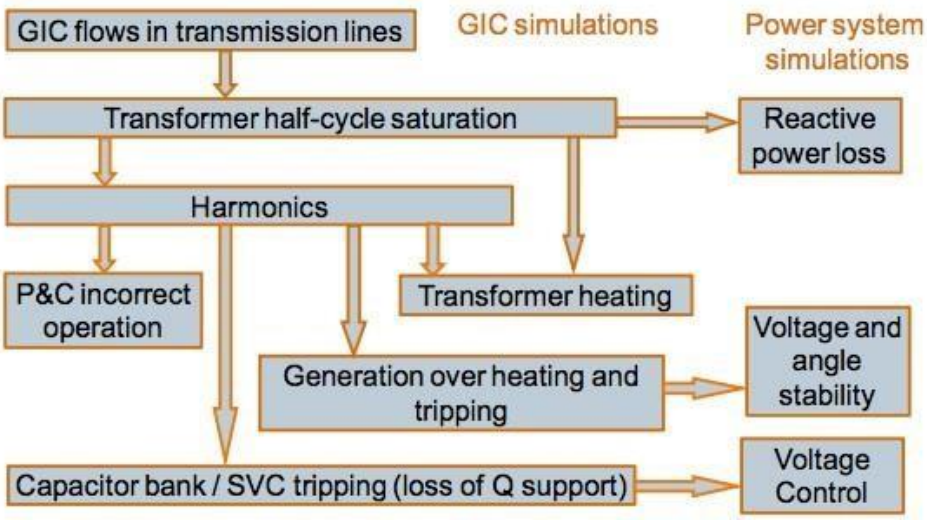

Figure 1-3 Potential effects of GICs on power system grid [7]

The vulnerability of the electric power transmission lines increases with the length of the electrical power transmission line. The Basis for calculating the voltage across a section of a power conductor is given by Equation 1.1

$$V_{AB}=\int E.dl \qquad 1.1$$

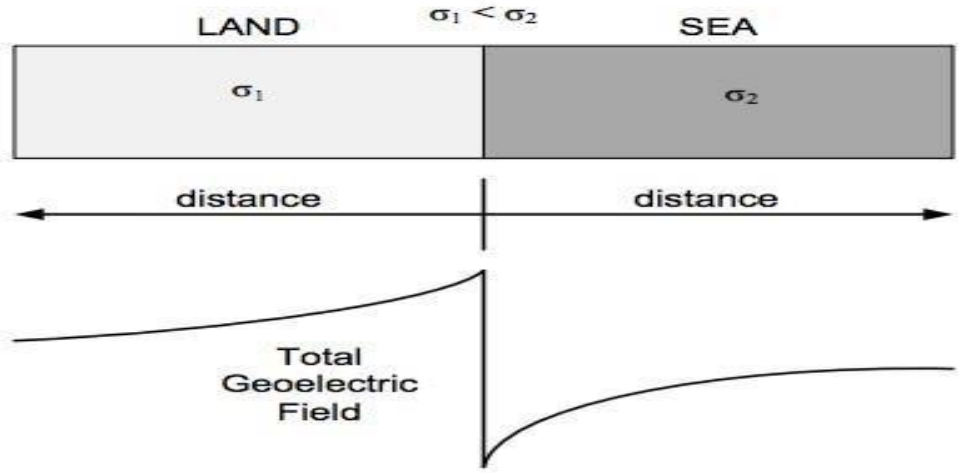

Figure 1-4 The geoelectric field tracing on field [8]

where V_{AB} is that the voltage between nodes A and B induced by the Electrical field E over a small line segment, e.g. a cable. If the electrical field E across the facility system is assumed to be

uniform then the voltage across the electrical transmission lines is found by integrating over straight lines between a node substation [8-9]. GICs may flow through any grounded component of the facility grid. But of all the results which will occur within the power grids thanks to solar storms, the results of GIC flowing through high voltage transformers are maybe the foremost severe ones and cause the best risk [9].

The transformer flux in the core is the sum of the DC flux and the AC flux, as shown in Equation 1.2. In the negative half- cycle, the DC flux are subtracted from the AC flux. While within the positive half-cycle the transformer core will enter saturation as shown in Figure 1-6 .which is called half-cycle saturation [11].

$$\Phi=\Phi_{AC}+\Phi_{DC} \qquad 1.2$$

The value of the DC flux depends on three main factors. The first one is the induced quasi-DC current, the second one is the number of turns in the transformer windings where the GIC current flows and the third one is the reluctance of the path of the DC flux [12-13]. This relation is shown in Equation 1.3

$$\Phi_{DC}= N*GIC/ \Re \qquad 1.3$$

where N is the number of turns, GIC is the geomagnetic induced current and lastly $\Re$ is the reluctance of the magnetic circuit. The reluctance $\Re$ is given by using Equation 1.4,

$$\Re= l/ \mu*A \qquad 1.4$$

where l is the length of the magnetic circuit,μ is the permeability of the material and A is the cross-sectional area of the circuit. Additionally, the reluctance $\Re$ is a function of the AC excitation. So, to find the magnitude of the flux Φ_{DC} one has to take into account an AC excitation and the level of saturation, and not only the GIC magnitude[14]. The significant increase of reactive power consumption is due to half-cycle saturation and cause significant flow of active and reactive power flow and intolerable system voltage problems.

GIC flowing in the transformer core lead to a higher magnetizing peak current, which produce a higher flux, that also contains a lot of harmonics. This leads to a large increase of eddy and circulating current losses in both windings and structural parts of the transformer, causing heat generation and transformer losses [15-16]. Because the GIC-imposed thermal duty is outside the

standard service parameters the increase in temperature and load losses of windings and structural parts

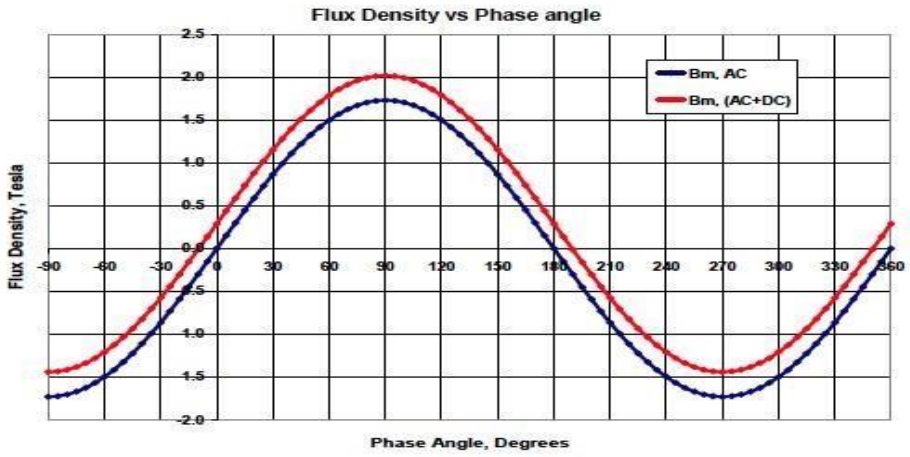

Figure 1-5 flux density shift in the core caused by DC [18-19]

Should be assessed individually for each type of power transformer design [17]. Several articles from the" IEEE Xplore Digital Library concludes that overheating due to induced DC-current should not necessarily have any bad impact on the reliability and quality of the power transformer. The reason is the period and frequency of the rate of GICs, which is too short to induce a critical temperature rise and low enough to give the transformer time to cool off, respectively [18]

The papers given in [18-19] summarizes the most high levels of GIC should not lead to damaging of transformer by overheating. The transformer core type and shell type are the exceptions. The researchers argue that some large significant overheating and winding damage caused by GICs, were found to be located in , or by system instability experienced during a GIC event. The published article in [19] proofs that the necessary condition to determine the possibility of transformer winding overheating due to high levels of GIC.

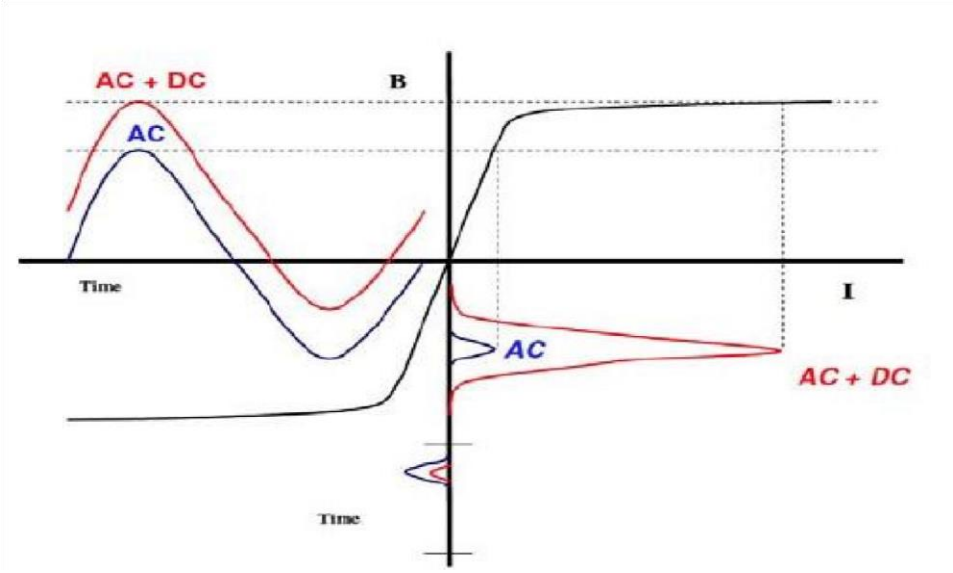

Figure 1-6 Part cycle semi-saturation of cores [18-19]

The DC flux shift from GICs in different core types leads to different magnitudes of peak magnetizing currents draw by the power transformer. Power transformers divided into two groups namely three-phase three-legged power transformers and core type transformer. Figure 1-7 shows the large three-phase three-legged transformer and a large single-phase transformer, respectively [20]. The peak magnetizing current drawn by the single-phase transformer is much larger than the peak magnetizing current drawn by the three-phase transformer for the same magnitude of GIC currents flowing in each transformer [18-19].

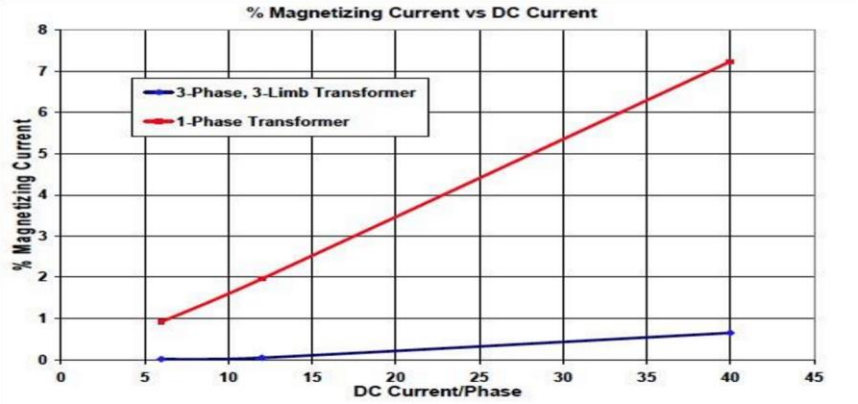

Figure 1-7 Magnetizing current for 3 phase and single-phase transformer [18-19]

Previously the power transformer manufacturing places has not been asked to give knowledge of transformer functionality and sensitivity against GICs. But in today modern days the specification of GIC tolerance levels for new transformers is usually included in the excel datasheet of the power transformer. Additional development should be carried out for to make a good choice of transformer and to consider the risks associated with GICs [22]

1.5. Scope and Significance of the Study

The scope of this thesis work is to investigate the effect of GIC on transformers and transmission lines using power world simulator software.

The geomagnetic disturbance field data recorded from the year 2012-2021 is used for the analysis of GIC in transformers and transmission lines. Such analysis GIC is useful for to identify the most severe latitude region of ethiopia affected by GIC.

The investigation carried out in this thesis is useful input for the Ethiopian Electric Power Corporation. Moreover, this research may be used as a reference for the researchers and help to further study and propose possible mitigation techniques for protecting electrical power system such as transformers and transmission lines from GIC.

1.6. Research Methodology

Calculation of GIC in an electrical power network basically includes two parts

a) Determine the electromagnetic field induced by magnetospheric-ionospheric currents. In this part, we should obtain the ground electrical conductivity and magnetospheric-ionospheric currents in the region.

b) Determine GIC in power grid. The network topology resistances and geoelectric data should be known.

When ground electric field is known, it can be equivalent for the voltage source for the network; the calculation of GIC is equivalent for the circuit problem. Therefore, the calculation of the GIC lies mainly in the first part. In theory, as long as we know the magnetospheric - ionospheric currents and earth conductivity distribution, GIC can be calculated. But in practice, magnetospheric - ionospheric currents and the earth conductivity model is hard to obtain, so we need to use some methods to simplify the calculation model.

a) **Plane Wave Method**:-Assuming the earth as a half infinite space of uniform conductivity, the relationship between components of electric field x , y and magnetic field y , x and the component in the time domain is shown as follows[22-23]

$$E(t) = -\frac{1}{\sqrt{\pi\mu_0\sigma}} \int_0^{\infty} \frac{g(t-u)}{u} du \quad 1.5$$

$$I = \frac{dB_x(t)}{t} \quad 1.6$$

Where, μ_0 = vacuum magnetic permeability

σ = earth conductivity

g(t-u) = time conductivity function

$B_x(t)$ = magnetic field function in time with x direction

I = current induced in the conductor

Assuming that the earth is a one-dimensional layered model, we only consider the earth conductivity changing with depth, ignoring the change in horizontal direction, the ground induced electric field in the frequency domain is:

$$E_x = -\frac{Z}{\mu_0} B_y \quad 1.7$$

Where, μ_0 = vacuum magnetic permeability

B_y = magnetic field component in y direction

Z = Surface wave Impedance

The surface wave impedance Z can also be calculated according to recursive formula [23] . The plane wave method is relatively simple, so good accuracy can be achieved in low latitudes, but as ignoring the lateral changes of the earth conductivity, so this method may cause larges errors in regions with mutational conductivity.

a) Complex Image Method (CIM) When calculating the GIC, we usually assume that the earth is a one-dimensional model of horizontal slice, the electrical conductivity is only

related to the depth. Complex image method is a approximation algorithm of precise formula. This method simplify the earth into an equivalent ideal conductor deeply p from ground. Ground electromagnetic field can be considered as the superposition of electromagnetic fields generated by current and its plane mirror symmetrical about ideal conductor. P is a plural, known as the complex table depth, it can be calculated by formula [24] .

$$P = \frac{z}{j\omega\mu_0} \qquad 1.8$$

Where, P = complex table depth

μ_0 = Vaccum magnetic permeability

Z = Surface wave impedance

The surface wave impedance Z can be calculated according to recursive formula in literature [25-26] . CIM enables fast and accurate computations, so this method has been widely used in the calculation of GIC. But it is worth noting that the complex image method applies only to one dimensional earth conductivity model of horizontal uniform, in coastal areas, the vast difference between the soil and water conductivity damage the uniformity on the horizontal direction, the complex image method is not applicable to such areas.

GIC power flow methodology: -Consider a standard m bus power flow model (e.g., positive se-quince) in which the m buses are grouped into s substations; let n=m+s. Because the GICs are considered to be DC , how they flow through the power grid can be determined by solving bthe following equation equation

$$V=G^{-1}I \qquad 1.9$$

where G is n by n symmetric matrix similar in form to the power system bus admittance matrix, except 1) it is a real matrix with just conductance values,2)the conductance values are determined by the parallel combination of the three individual phase resistances, 3) is augmented to include the substation neutral buses and substation grounding resistance values, 4) transmission lines with series capacitive compensation are omitted since series capacitors block dc flow, and 5) the transformers are modeled with their winding resistance to the substation neutral and in the case of

autotransformers both the series and common windings are represented. Of course for large systems is quite sparse and hence can be solved with computational effort equivalent to a single power flow iteration[25-26]

When solved the voltage vector contains entries for the s substation neutral DC the vector models the impact of the GMD-induced electric fields as Norton equivalent DC current injections. Two main methods have been proposed for representing this electric field variation in the power grid: either as dc voltage sources in the ground in series with the substation grounding resistance or as dc voltage sources in series with the transmission line resistances voltages and the m bus DC voltages. In both approaches Thevenin equivalent voltages are converted to Norton equivalent currents only the transmission line approach can handle the non-uniform electric fields that would be expected in a real GMD event. This is the approach used in this paper. Using the approach of [26], to calculate the GMD-induced voltage on transmission line k, the electric field is just integrated over the length of the transmission line as shown in the equation 1.10

$$U_k = \int_R \overrightarrow{E} . d\vec{l} \qquad 1.10$$

.

Where, R = geographic route of transmission line k

$\overrightarrow{E}$. = The Electric Field along the transmission line k

$d\vec{l}$ = is the incremental line segment

U_K = is the voltage induced along two transmission line

If the electric field is assumed to be uniform over the route of the transmission line then it is path independent and can be solved by just knowing the geographic location of the transmission line's terminal buses.

So in general after the DC Analysis to get the GICs, then I determined the effect of those GICs on the network and one of the most important aspect is their increase in reactive power, the cause of increase of reactive power on the transformer and how that increased in the transformer is determined by computing an AC network modelling which is an AC calculations power flow analysis can be done using power world simulator software and python

1.7. Organization of Thesis

Chapter 1 gives a general introduction of the study, statements of the problem, the objectives and the research methods and procedures used for this thesis. Chapter 2 focuses on the literatures review. Chapter 3 focused on Network Models, Simulation Studies and analysis of results chapter 4 discusses Conclusions, Recommendations and Future Work. Finally, a list of bibliographies used, and appendices of network data are provided at the end.

Chapter 2

Analysis of Geomagnetic Induced Current in Electric Power Systems

2.1 Introduction

Due to the interaction between the coronal mass ejections and the earth magnetosphere a powerful surge of electrical current induced in the ionospheric region and this powerful surge of electrical current accumulation on the ionosphere termed as Geomagnetic Induced Current. On the other hand, in the ionospheric region there is a magnetopause region, which is boundary to separate the earth atmosphere and the coronal mass ejections but due to this magnetopause inability to protect the earth atmosphere from GIC, its boundary is stretched to the direction of earth magnetic field and allow GIC to flow to the earth atmosphere.

Scientists uses the stretching of the boundary of the magnetopause to make analysis of the GIC by using plane wave model. The Plane wave model analysis is ignoring the curvature of the earth surface analysis and used cartesian coordinate system analysis. The cartesian coordinate system uses the X and Y coordinate system to make analysis of the resistivity in the electrical substations. To assess the geomagnetic hazard to power systems, it requires the ability to simulate the geomagnetically induced currents (GIC) flowing in the power network.

The first attempts of modelling GIC started by using power system modelling tools such as the Electromagnetic Transients Program. Later, Lehtinen & Pirjola developed a stand-alone method of calculating GIC in Electrical Power System that has been widely used in the geophysics community and widely accepted by scientific community. In the Lehtinen & Pirjola method geovoltage V_{im} is produced by the horizontal geoelectric field E, which is external from the

viewpoint of the network in the engineering part of a GIC calculation. Thus, V_{im} is obtained by integrating E along the path defined by the conductor line from station i to station m (i, m = 1,..., N) as shown in equation 2.1

$$V_{im} = \int_n^m E.dS \qquad 2.1$$

2.1.1 Reason and Mechanisms of GIC occurrence

GIC Maps are presented as a geoelectric field amplitude and horizontal surface polarization for the GIC analysis. These map are shown in Figure 2-1 below and come from geoelectric statistical field calculated for large and small sites across the Northeast high latitude region of ethiopia by frequency domain multiplication of 172 magneto-telluric impedance tensor and acquired during an intense survey, with decades-long, 1-min resolution.

Magnetically enhanced equatorial electro jet current produced by the sun's radiation gives the unique medium for a large dynamo-generated atmospheric current system magnifying the solar quiet daily variations (Sq.), the lunar quiet day variations and solar flare effects. This large concentration of electric current flowing from west to east in a small belt flanking the dip equator on the western and southern hemisphere termed as the equatorial electrojet and this equatorial electrojet current is the main reason for the creation of GIC. The overhead current system has been found to be localized in latitudinal and longitudinal width to a very small belt of about 600 km, at 75% peak value but centered at the dip equator in both in northern and southern hemisphere, and at an altitude of about 100 km. This width is also observed to different places over the earth and the variation has been associated with the difference in the rate of change of dip angle with latitude. on statistic of geomagnetic variation are acquired at different magnetic. Basically there are two mechanisms in which GIC occurs [26-27] which are the fluctuating ionospheric current system associated with the equatorially displaced auroral-electro jet and the temporal variation in the boundary of the magnetopause region.

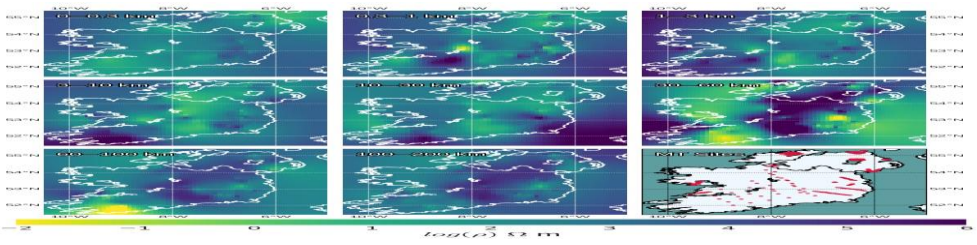

Figure 2-1 Resistivity of various depth intervals in the geology structure down to 200 km given by our MT model for different km for the intended transmission line [26-27].

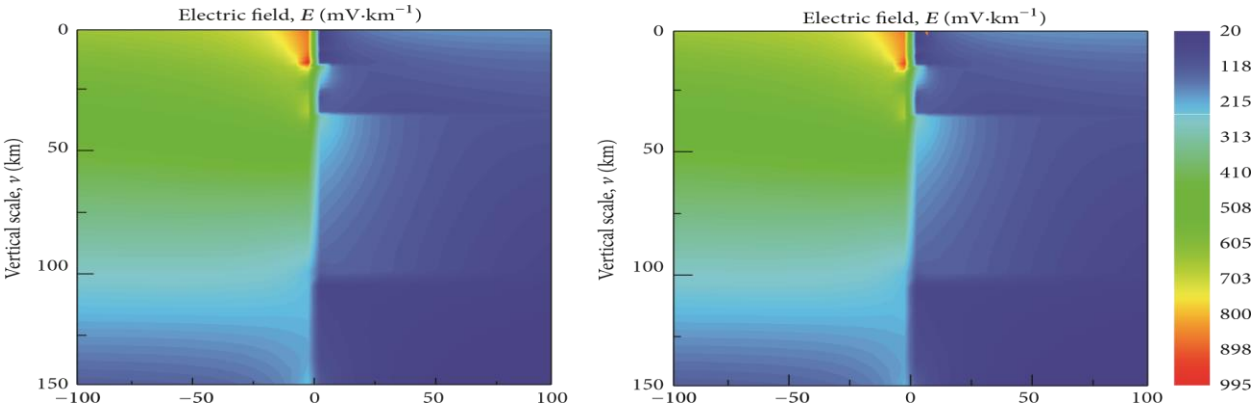

Figure 2-2 Contour diagrams of induced currents and electric fields results from 2D FEM for the geomagnetic induced current on the power network [28].

2.1.2 Method of Analysis of Geomagnetic Induced Current

a) Geophysical analysis

The Geophysical Analysis GIC includes determination of the horizontal geoelectric field at Earth's surface, Determination of symmetric disturbance field or (SYM-H) index, Determination of AU (eastward electrojet) and AL (westward electrojet) indices using 1 min resolution data. Eq. 2.2 was used to obtain the geomagnetic field derivatives.

$$\frac{dB}{dt}=\sqrt{\left(\frac{d_{B_x}}{dt}\right)^2+\left(\frac{d_{B_y}}{dt}\right)^2} \qquad 2.2$$

Where, B = Total magnetic field

d_{B_x} = The magnetic field derivative in x direction

d_{B_y} = The magnetic field derivates in y direction

The symmetric disturbance field or (SYM-H) Index for Ethiopia is measured from 2012-2021 and also the eastward electrojet and the westward electrojet indices data is collected from Addis Ababa geomagnetic observatory.

Therefore, The Geophysical Analysis of GIC consists of the earth ground conductivity analysis and earth surface geomagnetic data analysis.

The geomagnetic data consists of ionospheric-magnetospheric current data, The symmetric disturbance field or (SYM-H) Index data and the eastward electrojet and westward electrojet indices data.

b) Engineering Analysis

The Engineering Analysis of GIC is basically a circuit problem and also GIC is treated as quasi-DC currents because of its low frequency behavior. Therefore, the engineering analysis of GIC consists of the electrical circuit network network topology and geoelectric data.

The electrical circuit network topology given in figure 2-3 can be computed by the power network data and consists of :

- ✓ Coordinates of the substations in latitude and longitude value
- ✓ Total earthing resistances consists of transformer resistance, station earthing resistance an Resistance of possible neutral point reactor or resistor
- ✓ Transmission line resistances
- ✓ Network topology and configuration (locations of the lines)
- ✓ Precise information of the connections at the station (Autotransformers, transformer, buses etc...)

Geo-voltage U_{mn} produce in the electrical transmission line L between substations m and n is the line integral of the geoelectric field E along L and is given by equation 2.3 below.

$$U_{mn} = \int_m^n E * dl \qquad 2.3$$

E is rotational. Thus, no "(geo) potential" or "Earth surface potential" or "potential difference between lines" exists, and the line integral of E depends on the integration path L only

Where,

$$E = -\nabla\emptyset - \frac{\partial A}{\partial t} \qquad 2.4$$

Both the first (scalar potential) term and the second (vector potential) term given in equation 2.4 are important contributions to E. generally the basic formula for GIC in an N-node network is given by the new LP method in Eq. 2.5

$$I_e = (1+Y_nZ_e)^{-1} \qquad 2.5$$

Where

I_e = N×1 matrix of GIC into the Earth at the nodes

1 = N×N unit matrix

Y_n =N×N network admittance matrix determined by line resistances

Z_e =N×N earthing impedance matrix affected by earthing resistances

J_e = N×1 matrix involving the effect of geo-voltages

.

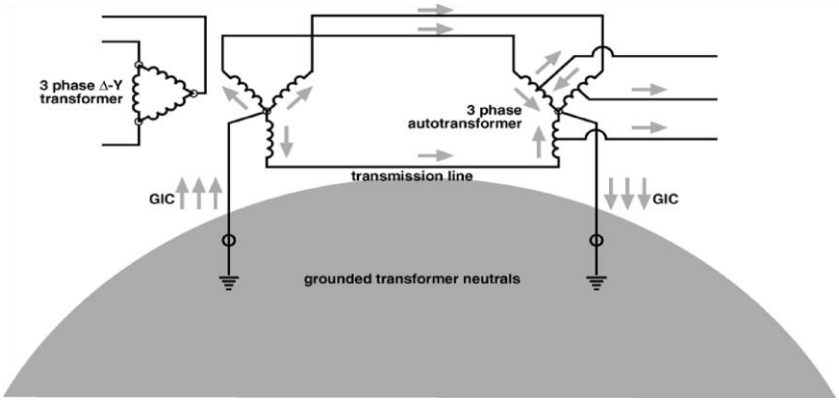

Figure 2-3 Propagation of GIC through the ground transformer neutral [29]

2.1.3 Vulnerability Assessment of Transformer and Transmission line due to Geomagnetic Induced current

In power system modelling, "vulnerability" has been a main and vital topic in the study of complex electrical power networks [14, 15,16]. The vulnerability of line is defined to be the reduction in the level of network performances after the line is removed intentionally from the particular network. This topics has its origin within the electrical power research on complex networks [17], and has been introduced into the study on most complex networks to assess from different perspective. The objective is to see the crucial critical and main faults happening the during the operation of the power system network and thus it needs more and necessary actions for preventions and adjustments.

Performance Index (PI) was first proposed to evaluate the transmission line loading and voltage performance for the automatic contingency selection algorithm [20]. Different vulnerability analysis techniques for power systems are used by different researchers. performance indices with contingency analysis in [22, 23, 24], transient energy function method is employed in [25], a

quick sensitivity type algorithm in [26], and many mores in [27, 28,29].During Geomagnetic Induced current analyzing an in depth data set, the direction of the geoelectric field and geomagnetic field is slightly increase in east-west than north-south oriented, but higher north-south geoelectric fields may occur also at a certain point.

Thus, the vulnerability assessment of high GIC are often induced during a cable having any direction and angle in addition to this , GIC flowing through a transformer is always the sum of GIC induced in several transmission lines having different directions and angle during the Vulnerability Assessment method of the power network this indicate that we should always not or believe the directions and of transmission lines when evaluating the likelihood of GIC problems.

Chapter 3

Modelling of Ethiopian Power System Network and Simulation Studies.

3.1 Introduction

In this chapter, a brief introduction to the tool used for the modelling and simulation, power world software integrated with python programming language is given in section 3.2; thereafter the Geo electric field modelling of transformers and transmission lines is presented in section 3.3 and finally the simulation and result analysis for the transformers and transmission lines in Ethiopian electric power network for the selected area is presented in section 3.4

3.2 Power World Software

Power world software integrated with python is designed as to investigate the geomagnetic induced current and other space weather phenomena in order to make a real time simulation to show its effect in power system model. The power world software tool key feature includes: -

1. Modification and organization of cases, numerical routines, output and documentation functions.

2. Integrated interactive single and multiple line graphic and data processing

3. Power system elements

4. Integrated calculation functions (e.g. line and machine parameter calculation based on geometrical or nameplate information).

5. Generic interface for computer-based mapping systems

6. Analysis of geomagnetic induced current with Electric Field values.

7. Security Constraint Optimal Power Flow (SCOPF)

8. Available Transfer Capability (ATC)

7. Optimal Power flow Reserves etc…

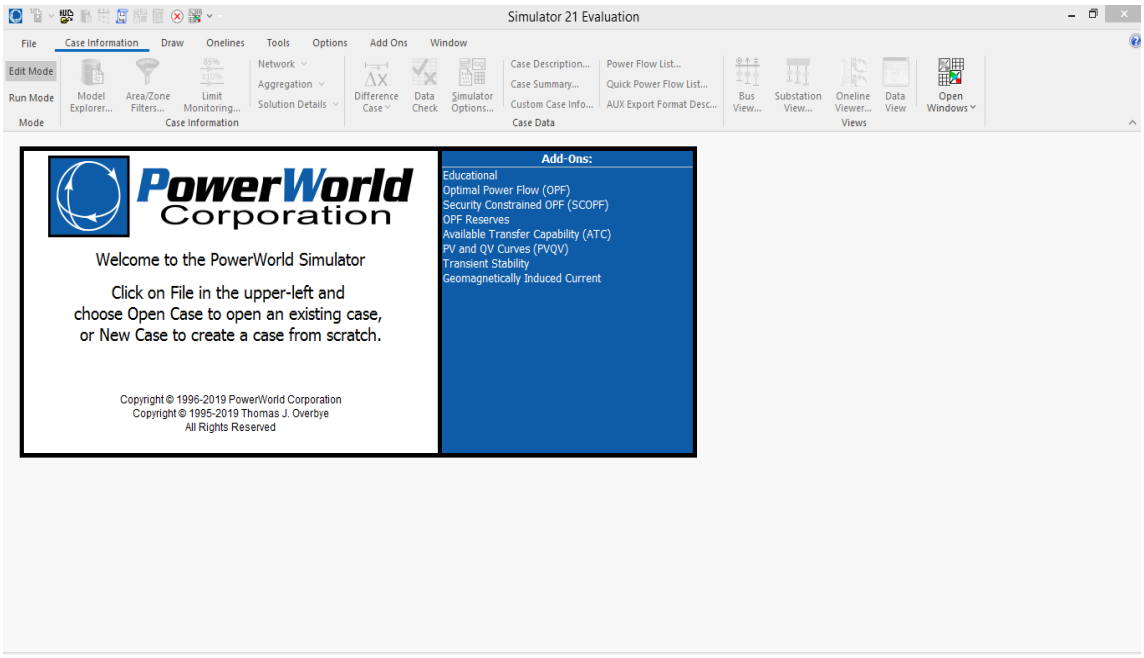

Figure 3-1 Power world software tool

The GIC analysis tool in power world simulator is an integral part of the power flow analysis that can be performed in the simulator. The module gives the user to simulate a geo-magnetic storm with a particular electric field and magnetic field value. From the GIC module in power world software is possible to determine reactive power losses in the transformer c

It is also possible to use information gathered by simulation and use it for power flow simulations in power world simulator.

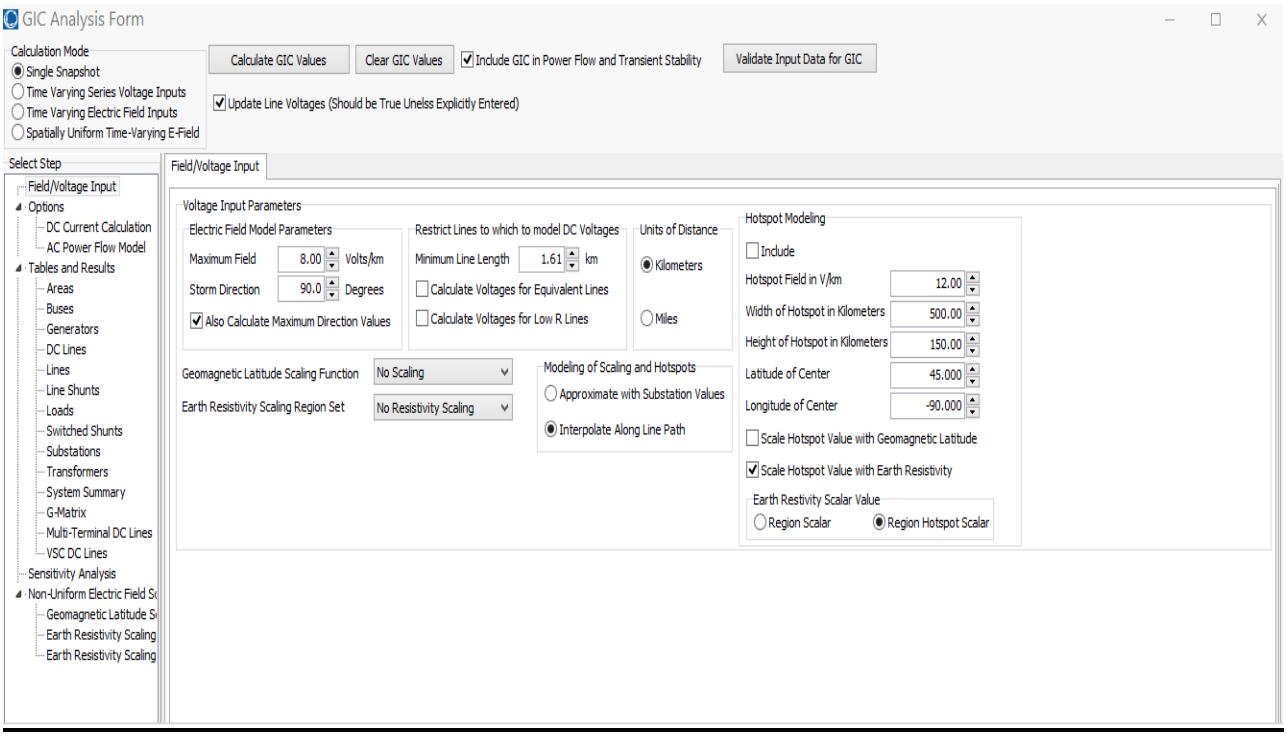

Figure 3-2 GIC analysis window

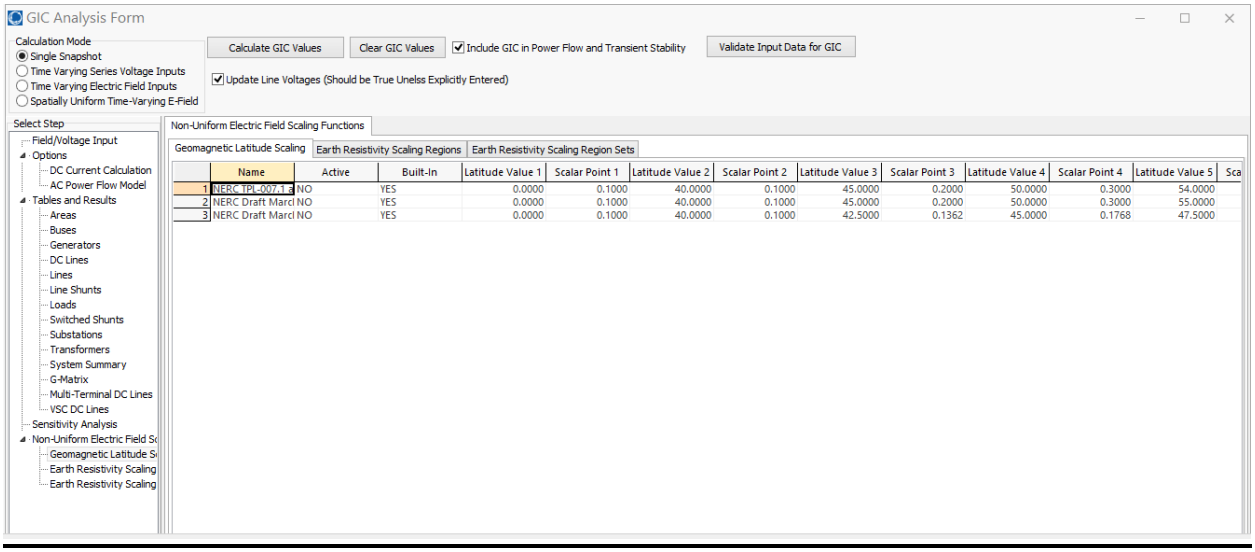

Figure 3-3 Geomagnetic latitude parameters

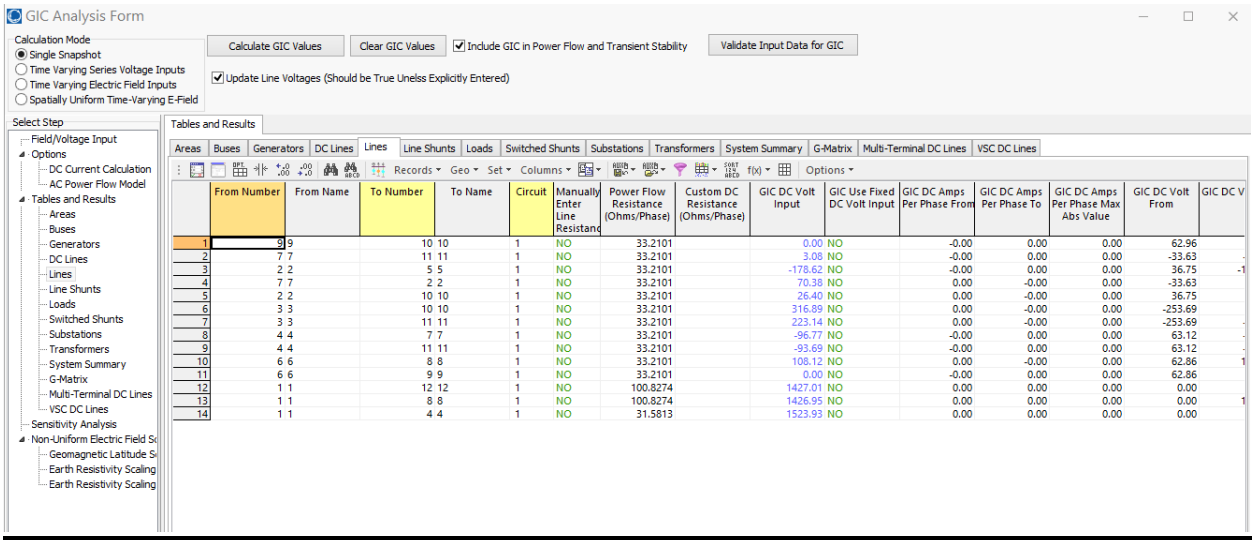

Figure 3-4 Bus value parameters

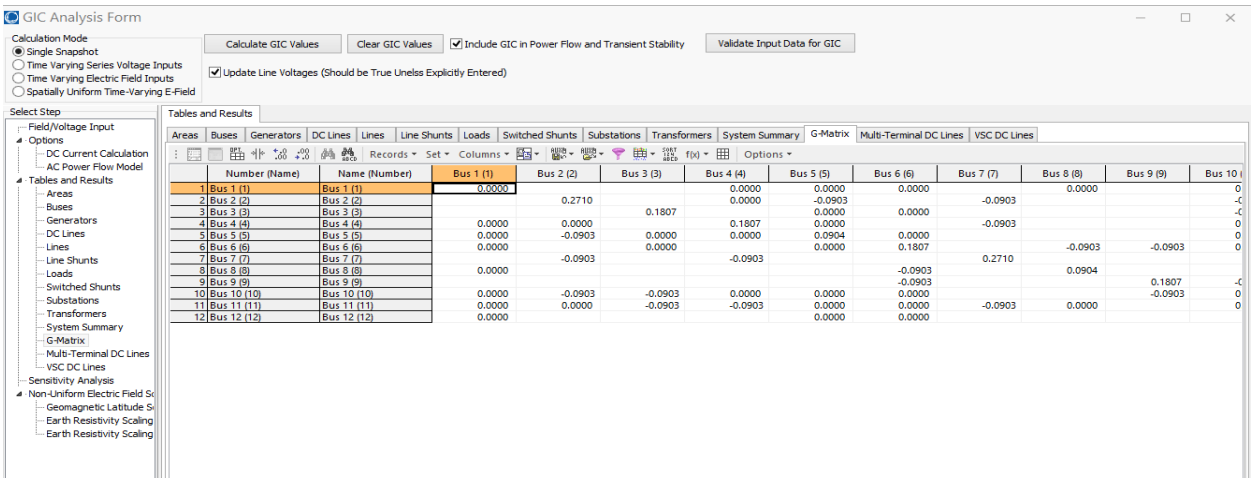

Figure 3-5 G-matrix parameters

3.3 Geoelectric Field Modelling of Ethiopian Power Systems

The frequency-dependent (ω) plane-wave equation which tells about the relationship between horizontal electric field and magnetic field components at a substation surface and is given by

$$E(\omega) = Z(\omega)\, B(\omega) \qquad 3.1$$

Where $E(\omega)$ = the electric field value as a function of frequency

$Z(\omega)$ = the Impedance tensor value as a function of frequency

$B(\omega)$ = the magnetic field value as a function of frequency

$$\begin{pmatrix} \frac{E_x}{E_y} \end{pmatrix} = \frac{1}{\mu_o} \begin{pmatrix} Z_{xx} & Z_{xy} \\ Z_{yx} & Z_{yy} \end{pmatrix} \begin{pmatrix} B_x \\ B_y \end{pmatrix} \quad 3.2$$

Where Z is the impedance tensor, and μ_0 is the vacuum permeability

$$Z_{1D} = \begin{pmatrix} 0 & Z_{xy} \\ -Z_{xy} & 0 \end{pmatrix} \quad 3.3$$

This sets the parallel elements (Z_{xx} and Z_{yy}) to zero as lateral changes are ignored, leaving only the off-diagonal elements Z_{xy}. The electric field components can then be written as

$$E_x(\omega) = \frac{1}{\mu_0} Z_{xy}(\omega)\, B_y(\omega) \quad 3.4$$

Where $E_x(\omega)$ = the x component value of the Electric Field as the function of frequency

$Z_{xy}(\omega)$ = the two-dimensional impedance tensor value as the function of frequency

$B_y(\omega)$ = the y component value of the magnetic field as the function of frequency

μ_0 = the Vacuum Permeability

$$E_y(\omega) = \frac{-1}{\mu_0} Z_{xy}(\omega)\, B_x(\omega) \quad 3.5$$

There is a frequency dependent equations which were used in this thesis to calculate the electric field and magnetic field when coupled with the MT derived multi-layered earth resistivity model and given from equation 3.6 to 3.9

$$E_{x1y1}(t) = \frac{1}{\sqrt{\pi \mu_{0\sigma}}} \int_0^{\infty} \frac{1}{\tau} \frac{dB_{yx1(t-\tau)}}{dt} d\tau \quad 3.6$$

$$E_{x2y2}(t) = \frac{1}{\sqrt{\pi \mu_{0\sigma}}} \int_0^{\infty} \frac{1}{\tau} \frac{dB_{yx2(t-\tau)}}{dt} d\tau \quad 3.7$$

$$E_{x3y3}(t) = \frac{1}{\sqrt{\pi \mu_{0\sigma}}} \int_0^{\infty} \frac{1}{\tau} \frac{dB_{yx3(t-\tau)}}{dt} d\tau \quad 3.8$$

$$E_{x4y4}(t) = \frac{1}{\sqrt{\pi \mu_{0\sigma}}} \int_0^{\infty} \frac{1}{\tau} \frac{dB_{yx3(t-\tau)}}{dt} d\tau \quad 3.9$$

where dB/dt is the varying magnetic field component perpendicular to E, τ is a time and σ is a earth conductivity value.

Then by adding each equations from 3.6 to 3.9 we get the following relations given below in equation 3.10 to 3.11

$$E_{xy=}E_{x1y1}(t) + E_{x2y2}(t) + E_{x3y3}(t) + E_{x4y4}(t)$$

$$= \frac{1}{\sqrt{\pi\mu_{0\sigma}}}\int_0^{\infty}\frac{1}{\tau}\frac{dB_{yx1(t-\tau)}}{dt}\,d\tau + \frac{1}{\sqrt{\pi\mu_{0\sigma}}}\int_0^{\infty}\frac{1}{\tau}\frac{dB_{yx2(t-\tau)}}{dt}\,d\tau + \frac{1}{\sqrt{\pi\mu_{0\sigma}}}\int_0^{\infty}\frac{1}{\tau}\frac{dB_{yx3(t-\tau)}}{dt}\,d\tau + \frac{1}{\sqrt{\pi\mu_{0\sigma}}}\int_0^{\infty}\frac{1}{\tau}\frac{dB_{yx3\,(t-\tau)}}{dt}d\tau \quad \ldots\ldots\ldots\ldots \quad 3.10$$

$$= \frac{1}{\sqrt{\pi\mu_{0\sigma}}}\left(\int_0^{\infty}\frac{1}{\tau}\frac{dB_{yx1(t-\tau)}}{dt}d\tau + \int_0^{\infty}\frac{1}{\tau}\frac{dB_{yx2(t-\tau)}}{dt}d\tau + \int_0^{\infty}\frac{1}{\tau}\frac{dB_{yx3(t-\tau)}}{dt}d\tau + \int_0^{\infty}\frac{1}{\tau}\frac{dB_{yx3(t-\tau)}}{dt}d\tau\right) \quad 3.11$$

A CME diffusion equation for E_y is derived from Maxwell's equations in Cartesian coordinates and is given by below in equation 3.12

$$\nabla^2 E_y = i\omega\mu_0\sigma E_y \quad 3.12$$

Where $\nabla^2 = \frac{\partial^2}{\partial x^2} + \frac{\partial^2}{\partial z^2}$ 3.13

$E_y = e^{\zeta z}\cos \nu x$, is valid only for a line current system and substituted into Eq. 3.13 to give

$$\left[\frac{\partial^2}{\partial x^2} + \frac{\partial^2}{\partial z^2}\right](e^{\zeta z}\cos \nu x) = [-\nu^2 + \zeta 2]\,(e\zeta z\,\cos\nu x) = i\omega\mu_0\sigma\,(e\zeta z\,\cos\nu x) \quad 3.14$$

Cancelling the general solution on both sides leads to the relation $\zeta 2 = \nu 2 + i\omega\mu_0\sigma$. The two roots of this equation would result in both an incident ($e^{-\zeta z}$) and a reflected ($e^{+\zeta z}$) wave for GIC propagation.

The geoelectric field elementary general solution including the incident ($e^{-\nu z}$) and reflected ($Re^{\nu z}$) parts of equation 3.14 with an arbitrary constant C and given by

$$E\,y(x,z;\nu,\omega) = C[e^{-\nu z} - R(\nu,\omega)e^{\nu z}]\cos \nu x. \quad 3.15$$

The reflection coefficient $R(\nu, \omega)$ and the electric field E_y also depends on the Earth's conductivity and given by equation 3.16

$$E_y(x,\omega) = i\omega\frac{\mu_0}{2\pi}\int_0^{\infty} J\nu(\nu,\omega)\,e^{-\nu h}[R(\nu,\omega) - 1]\cos(\nu x)\,\nu^{-1}\,d\nu \quad 3.16$$

$J\nu(\nu,\omega) = \int_{-\infty}^{\infty} j(x,\omega)e^{-i\nu x}dx$ is the Fast Fourier transform of the current density for a distribution of currents $j(x, \omega)$ in the real x space direction in the high latitude region.

$$\begin{bmatrix}B_x\\B_Y\end{bmatrix}(x,\omega) = \frac{\mu}{2\pi}\int_0^{\infty} J(\omega)\,e^{-\nu h}\begin{bmatrix}\{R(\nu,\omega)+1\}\cos(\nu x)\\\{R(\nu,\omega)+1\}\sin(\nu x)\end{bmatrix}d\nu \quad 3.17$$

Where

$$R\,(\nu,\omega) = \frac{i\omega\mu 0/\nu - Z(\nu,\omega)}{i\omega\mu 0/\nu + Z(\nu,\omega)} = \frac{i\omega\mu 0 - \nu Z(\nu,\omega)}{i\omega\mu 0 + \nu Z(\nu,\omega)}$$

where μ_0 is the free space permeability, ω is the angular frequency, and ν is the horizontal wave number.

Table 3-1 below shows the geomagnetic latitude value and its corresponding scaling factor.The scaling factor also know as the bench mark factor which is an essential value used in the geo-magnetic field modelling.

Table 3-1 Geomagnetic latitude value and its corresponding scaling factor

Geomagnetic Latitude (Degrees)	Scaling Factor1 (α)
≤ 40	0.10
45	0.2
50	0.3
54	0.5
56	0.6
57	0.7
58	0.8
59	0.9
≥ 60	1.0

$$E_y(x,\omega) = i\omega\frac{\mu_0}{2\pi}\int_0^\infty J\nu(\nu,\omega)\, e^{-\nu h}[R(\nu,\omega) - 1]\cos(\nu x)\, \nu^{-1}\, d\nu \qquad 3.19$$

Reduced to simple equation

$$E_{peak} = 8 \text{ x } \alpha \text{ x } \beta_b \text{ (V/km)} \qquad 3.20$$

$$E_{peak} = 12 \text{ x } \alpha \text{ x } \beta_s \text{ (V/km)} \qquad 3.21$$

Where: - α = the scaling factor to account for local geomagnetic latitude

β = a scaling factor to account for the local earth conductivity structure

Subscripts b and s for the β scaling factor denote association with the benchmark or supplementa l GMD events, respectively.

$$\alpha = 0.001 \text{ X } e^{(0.015\, x\, L)} \qquad 3.22$$

Where L is the geomagnetic latitude in degrees and $0.1 \leq \alpha \leq 1$.

One-dimensional layered earth resistivity model for Ethiopian Area

Table 3-2 One dimensional layered earth resistivity model for ethiopian area

Earth resistivity	Depth value
0.02	0.1
0.00002	8
0.005	31
0.01	100
0.001	∞

Table 3-3 One-dimensional layered earth resistivity model for Ethiopian area

Parameter	symbol	Value
Equatorial radius	A	6378.137 km
Polar radius	B	6356.752 km
Eccentricity squared	C^2	0.00669437999014km

$$L_N = \frac{\pi}{180} M.\Delta lat \qquad 3.23$$

where M is the radius of curvature in the high latitude region of ethiopia and is given by equation 3.23 below.

$$M = \frac{a(1-e^2)}{(1-e^2 sin^2\varphi)1.5} \qquad 3.24$$

Substituting the values from Table 3-3 gives the expression given below in equation 3-25

$$L_N = (111.133 - 0.56\cos(2\varphi))) \ .\Delta lat \qquad 3\text{-}25$$

Where Δlat is the difference in latitude (degrees) between the two Transmission line A and B, and φ is the average of the latitudes A and longitude B:

$$\varphi = \frac{LatA+LongB}{2} \qquad 3\text{-}26$$

Where LatA = latitude position of transmission line A

$_{LongB}$ =longitude position of transmission line B

Similarly, the East-West distance is given by:

$$L_N = \frac{\pi}{180} N\cos\varphi.\Delta long \qquad 3\text{-}27$$

where N is the radius of curvature in the plane parallel to the meridian as defined in Eq. 3-26 and Δlong is the difference in longitude (degrees) between the two substations A and B

$$N = \frac{a}{\sqrt{1-e^2 sin^2 \varphi}} \qquad 3\text{-}28$$

Substituting the values from Table 2 gives the following expression for the East-West distance in km:

$$L_E = (111.5065 - 0.1872\cos(2\varphi))).\cos\varphi \ .\Delta long \qquad 3\text{-}29$$

From the above equation 3-29, $L_N = (111.133 - 0.56\cos(2\varphi))) \ .\Delta lat$ and $L_E = (111.5065 - 0.1872\cos(2\varphi))).\cos\varphi \ .\Delta long$ are used to determine the voltage source in the transmission line to be used in the GIC modelling

The relations used to calculate distance from one degree of latitude and longitude is as

Follows:

1^o latitude = 111.133 - 0.560*cos (2ø) km

$$1^o \text{ longitude} = \frac{111.32\cos(ø)}{\sqrt{\sqrt{1-.\ 669\ \sin(ø)^2}}} \text{ km}$$

Where $\varphi = \frac{LatA+LongB}{2}$ 3-30

Lat A = latitude position of transmission line A

Long B = longitude position of transmission line B

$\varphi =$ angle in degree

Table 3-4 Line and geographic coordinate data

Node 1	Node 2	Network Level	l [km]	r [Ω/km]	x [Ω/km]	c [nF/km]	Ith [kA]	r0 [Ω/km]	x0 [Ω/km]	c0 [nF/km]	Geographic Coordinate in Degree
GG OLD 230 kV	Wolkite 230kV	230	65.3	0.0597	0.4113	8.9	1.05	0.2029	1.3029	6	8 lat 37 long
Gefarsa 132 BB1	Kaliti 132 BB1 I	132	24.75	0.1906	0.434	8.4	0.49	0.3724	1.3217	5.6	8.89 lat 38.7 long
Gefarsa 132 BB1	Sebeta I 132 TP	132	10.78	0.1906	0.434	8.4	0.49	0.3724	1.3217	5.6	8.54 lat 38.37long
MEKANISSA 132	Kaliti I 132 BB1	132	16.16	0.1906	0.434	8.4	0.49	0.3724	1.3217	5.6	8.98 lat 38.73 long
Sebeta I 132	Mekanissa 132	132	7.81	0.1906	0.434	8.4	0.49	0.3724	1.3217	5.6	8.92 lat 38.6268 long
Gefarsa 132 BB1	Addis North 132	132	11.11	0.1906	0.434	8.4	0.49	0.3724	1.3217	5.6	8.954lat 38.497long
Cotobie 132	Weregenu 132 TP	132	2.45	0.1906	0.434	8.4	0.49	0.3724	1.3217	5.6	9.02 lat 38.62 long
Weregenu 132 TP	Weregenu 132	132	4.5	0.1906	0.434	8.4	0.49	0.3724	1.3217	5.6	9.02 lat 38.62 long
Weregenu 132 TP	Kaliti I 132 BB1	132	17.51	0.1906	0.434	8.4	0.49	0.3724	1.3217	5.6	8.98 lat 38.73 long
Cotobie 132	Kaliti North 132 TP	132	18.65	0.1906	0.434	8.4	0.49	0.3724	1.3217	5.6	8.98 lat 38.6235 long

From the above data let change the geographic coordinate in to kilometer distance using equation 3.31

1^o latitude = 111.133 - 0.560*cos (2ø) km

$$\varphi = \frac{LatA+LatB}{2} \qquad 3\text{-}31$$

Case 1: GG OLD 230 kV and Wolkite 230kV:- 8 lat 37 long

$$\varphi = \frac{LatA+LongB}{2} = \frac{8\ lat+37\ long}{2} = 22.5^0$$

1^o latitude = 111.133 - 0.560*cos (2ø) km

= 111.133 - 0.560*cos (45) km

=110km

$$1^o \text{ longitude} = \frac{111.32\cos(ø)}{\sqrt{\sqrt{1-.\ 669\ \sin(ø)^2}}} = \frac{111.32\cos(22.5)}{\sqrt{\sqrt{1-.\ 669\ \sin(22.5)^2}}}$$

= 102.846 km

Geomagnetic storm of intensity 3.4 V/km uniform electric field aligned at a specific alligned

$$V_{Induced} = E \bullet L = E_x L_x + E_y L_y \qquad 3\text{-}32$$

Where , E_x = the Northward Electric Field Component

E_y = the Eastward electric Field Component

L_x = the Northward T_x Line distance.

L_y = the Northward T_x Line distance.

Lx = (8) * 110km =880km, L_y = (37)* 102.846km =3805.302km

$V_{Induced} = E \bullet L = E_x L_x + E_y L_y$ 3.33

= 3.4V/km* 880km +3.4V/km*3805.302km

=2292V+12,938.02V

= 15.23KV

Case 2: Gefarsa 132 BB1 and Kaliti I 132 BB1

1^o latitude = 111.133 - 0.560*cos (2ø) km

$$\varphi = \frac{LatA+LatB}{2} = \frac{8.89 + 38.7 \text{ long}}{2} = 23.795^0$$

111.133 - 0.560*cos (23.795) km

1^0 latitude = 110.62km

$$1^o \text{ longitude} = \frac{111.32\cos(ø)}{\sqrt{\sqrt{1-.\ 669\ \sin(ø)^2}}} = \frac{111.32\cos(23.795)}{\sqrt{\sqrt{1-.\ 669\ \sin(23.795)^2}}}$$

1^o longitude = 114.3km

L_x = (8.89)* 110.62km=983.411km

L_y = (38.7)* 102.846km=3980.14km

$V_{Induced} = E \bullet L = E_x L_x + E_y L_y$ 3.34

= 3.4V/km* 983.411km +3.4V/km*3905.14km

= 3,343.59V + 13,277.476V

=16.62KV

Case 3: Gefarsa 132 BB1 and Sebeta I 132 TP

$$\varphi = \frac{LatA+LongB}{2} = \frac{8.54 + 38.37\text{long}}{2} = 23.45^0$$

1° latitude = 111.133 - 0.560*cos (2ø) km

= 111.133 - 0.560*cos () km

=110.61km

$$1^o \text{ longitude} = \frac{111.32\cos(ø)}{\sqrt{\sqrt{1-.\ 669\ \sin(ø)^2}}} = \frac{111.32\cos(23.45)}{\sqrt{\sqrt{1-.\ 669\ \sin(23.45)^2}}}$$

= 114.23 km

L_x = (8.54) * 110.62km=110.61km

L_y = (38.37) * 102.846km=114.23 km

$V_{Induced} = E \bullet L = E_x L_x + E_y L_y$ 3.35

= 3.4V/km* 110.61km +3.4V/km*114.23 km

= 376.074V + 388.382V

=764.456V=0.7644kv

Case 4: MEKANISSA 132 and Kaliti I 132 BB1

$$\varphi = \frac{LatA+LongB}{2} = \frac{8.98 + 38.73\text{long}}{2} = 23.855^0$$

1° latitude = 111.133 - 0.560*cos (2ø) km

= 111.133 - 0.560*cos (47.71) km

=110.756km

$$1^o \text{ longitude} = \frac{111.32\cos(ø)}{\sqrt{\sqrt{1-.\ 669\ \sin(ø)^2}}} = \frac{111.32\cos(23.45)}{\sqrt{\sqrt{1-.\ 669\ \sin(23.45)^2}}}$$

= 114.23 km

L_x = (8.98)* 110.756km =994.588

L_y = (38.73)* 114.23 km =4424km

$$V_{Induced} = E \bullet L = E_x L_x + E_y L_y \quad (3.36)$$

$$= .3.4V/km * 994.588 + 3.4V/km * 4424km$$

$$= 3381 + 15041.6 = 18.42KV$$

Case 5. Sebeta I 132 and Mekanissa 132

$$\varphi = \frac{LatA + LongB}{2} = \frac{8.92 + 38.6268}{2} = 23.77$$

1^o latitude = $111.133 - 0.560 * \cos(2ø)$ km

$= 111.133 - 0.560 * \cos(47.54)$ km

$= 110.754$km

1^o longitude = $\frac{111.32 \cos(ø)}{\sqrt{\sqrt{1 - .\ 669 \sin(ø)^2}}} = \frac{111.32 \cos(23.77)}{\sqrt{\sqrt{1 - .\ 669 \sin(23.77)^2}}}$

$= 307.78$ km

$L_x = (8.92) * 1\mathbf{10}.754$km $= 994.588$

$L_y = (38.628) * 307.78$ km $= 4424$km

$$V_{Induced} = E \bullet L = E_x L_x + E_y L_y \quad (3.37)$$

$$= .3.4V/km * 994.588 + 3.4V/km * 4424km$$

$$= 3381 + 15041.6 = 18.42KV$$

Case 6: Gefarsa 132 BB1 and Addis North 132

$$\varphi = \frac{LatA + LongB}{2} = \frac{8.954\text{lat} + 38.497\text{long}}{2} = 23.72^0$$

1^o latitude = $111.133 - 0.560 * \cos(2ø)$ km

$= 111.133 - 0.560 * \cos(47.45)$ km

$= 110.754$km

$$1^o \text{ longitude} = \frac{111.32\cos(ø)}{\sqrt{\sqrt{1-.\ 669\ \sin(ø)^2}}} = \frac{111.32\cos(23.72)}{\sqrt{\sqrt{1-.\ 669\ \sin(23.77)^2}}}$$

$$= 307.78 \text{ km}$$

L_x = (8.92)* 1**10**.754km =994.588

L_y = (38.628)* 307.78 km =4424km

$$V_{Induced} = E \bullet L = E_x L_x + E_y L_y \qquad 3.38$$

=.3.4V/km* 994.588+3.4V/km*4424km

=3381+15041.6 =18.42KV

Case 7.0 Cotobie 132 and Weregenu 132 TP

$$\varphi = \frac{LatA+LongB}{2} = \frac{9.02 \text{ lat}+38.62 \text{ long}}{2} = 23.82$$

1^o latitude = 111.133 - 0.560*cos (2ø) km

= 111.133 - 0.560*cos (47.64) km

=110.755km

$$1^o \text{ longitude} = \frac{111.32\cos(ø)}{\sqrt{\sqrt{1-.\ 669\ \sin(ø)^2}}} = \frac{111.32\cos(23.82)}{\sqrt{\sqrt{1-.\ 669\ \sin(23.77)^2}}}$$

$$= 114.25 \text{ km}$$

L_x = (9.02)* 1**10**.755km =999.01

L_y = (38.62)* 114.25 km =4412.3km

$$V_{Induced} = E \bullet L = E_x L_x + E_y L_y \qquad 3.39$$

=.3.4V/km* 999.01+3.4V/km*4412.3km

=3396.64+15001.82 =18.39KV

Case 8. Weregenu 132 TP and Weregenu 132

$$\varphi = \frac{LatA+LongB}{2} = \frac{9.02 \text{ lat}+38.62 \text{ long}}{2} = 23.82^0$$

1º latitude = 111.133 - 0.560*cos (2ø) km

= 111.133 - 0.560*cos (47.64) km

=110.755km

$$1^o \text{ longitude} = \frac{111.32\cos(ø)}{\sqrt{\sqrt{1-.\ 669\ \sin(ø)^2}}} = \frac{111.32\cos(23.82)}{\sqrt{\sqrt{1-.\ 669\ \sin(23.77)^2}}}$$

= 114.25 km

L_x = (9.02)* 1**10**.755km =999.01

L_y = (38.62)* 114.25 km =4412.3km

$V_{Induced} = E \bullet L = E_x L_x + E_y L_y$ 3.40

=.3.4V/km* 999.01+3.4V/km*4412.3km

=3396.64+15001.82 =18.39KV

Case 9. Cotobie 132 and Kaliti North 132 TP

$$\varphi = \frac{LatA+LongB}{2} = \frac{8.98 \text{ lat} +38.6235 \text{ long}}{2} = 23.8^0$$

1º latitude = 111.133 - 0.560*cos (2ø) km

= 111.133 - 0.560*cos (47.6) km

=110.755km

$$1^o \text{ longitude} = \frac{111.32\cos(ø)}{\sqrt{\sqrt{1-.\ 669\ \sin(ø)^2}}} = \frac{111.32\cos(23.8)}{\sqrt{\sqrt{1-.\ 669\ \sin(23.8)^2}}}$$

= 114.31 km

L_x = (8.98 lat)* 1**10**.755km = 994.59 km

L_y = (38.6235 l)* 114.31 km =4415.0km

$$V_{Induced} = E \bullet L = E_x L_x + E_y L_y \quad (3.41)$$

$$= .3.4V/km * 994.59 + 3.4V/km * 4415.0km$$

$$= 3381.60 + 15011 = 18.3926KV$$

The transformer's operating region is between V+ to V-, with an rms voltage of 0.5 pu. For a given level of semi-saturation, V_{DC} is defiend by equation 3.42

$$V_{GIC}^{+} = V_{DC} + \sqrt{2} \quad (3.42)$$

$$V_{GIC}^{-} = V_{DC} - \sqrt{2}$$

Let we assuming that the transformer is operating in the semi saturated region given by equation 3.43 below.

$$V^{+} > V_{knee} \quad (3.43)$$

$$V_{knee} < V^{-} < V_{knee}$$

The current limits of the transformer's operating region is defined by I_{GIC}^{+} and I_{GIC}^{-} and given below in equation 3.44 and equation 3.45.

$$I_{GIC}^{+} = B_{aircore}\left((V_{DC}+\sqrt{2}) - \sqrt{2}\, V_{knee}\left(1 - \frac{B_m}{B_{aircore}}\right)\right) \quad (3.44)$$

$$I_{GIC}^{-} = B_m (V_{DC} - \sqrt{2}) \quad (3.45)$$

The effective susceptance of the electrical power transformer is given by equation 3.44

$$B_{effective} = \frac{I_{GIC}^{+} - I_{Gic}^{-}}{v_{GIC}^{+} - v_{Gic}^{-}} \quad (3.44)$$

The reactive power absorbed by the electrical power transformer is given by equation 3.45 and equation 3.46

$$Qtr = VI\sin\theta \quad (3.45)$$

$$= B_{effective} V^2 \quad (3.46)$$

3.4 Simulation Studies and Analysis of Results

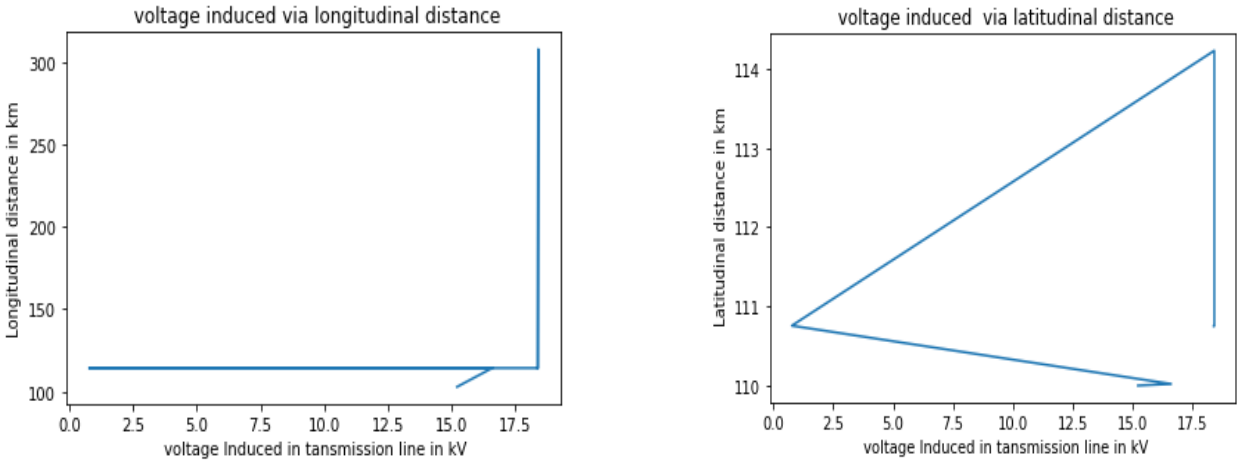

Figure 3-6 Voltage induced for different longitude and latitude value

As shown in the Figure 3-6 above the voltage induced in kV is different for different longitude and latitude value. One of the main reasons behind this difference in voltage for different longitude and latitude value is the directional sensitivity of geomagnetic disturbance field (Dst) and the equatorial electrojet magnetic field.

Ethiopia is located on the southern hemisphere (located 3′ and 14.8″ latitude 33′ and 48′ longitude) and because of the longitude and latitude value differences, the stretching of the magnetic field of the geomagnetic disturbance (Dst) and the magnetic field of the equatorial electrojet is different and this stretching of magnetic field induced different voltage in different value of longitude and latitude in the southern hemisphere, the hemisphere in which Ethiopia is located. .

According to **Longitudinal Voltage Induction theorem** the slope of the voltage wave form with their respective electric field value is given as follow below in table 3-5 below.

Table 3-5 Acceptable slope value for a high electro-jet longitude area

Electric field strength value in kV/km	Acceptable slope value for the voltage induced via longitudinal distance	Best Probable acceptable Value
3.4	0.3<m<0.6	0.4
3.5	0.6<m<0.8	0.7
3.6	0.8<m<0.9	0.85

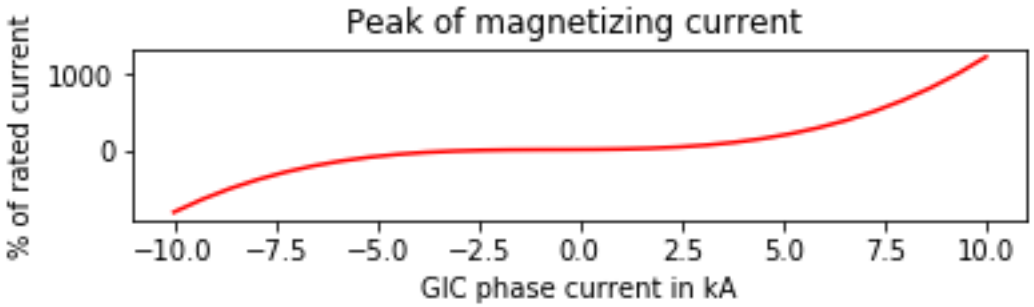

Figure 3-7 Peak magnetizing current for the transformer

Figure 3-7 shows magnetizing peak current or inrush current of the transformer. In this case the peak magnetizing current of a transformer is same as inrush current of the transformer and represented by GIC phase current. As we know from the fact that the inrush current of a transformer is 10 times higher than normal rated current of transformer but because of the GIC current is much greater than the rated current of the transformer, the percentage of GIC flowing in the electrical power transformer is approximately 1000 percent greater than the rated peak magnetizing current of the transformer. The simulation calculated the rated current of the transformer for the maximum of 200A but the percentage decrease as the rated current of the transformer decrease so to show the decreases of the current, it is represented as negative value.

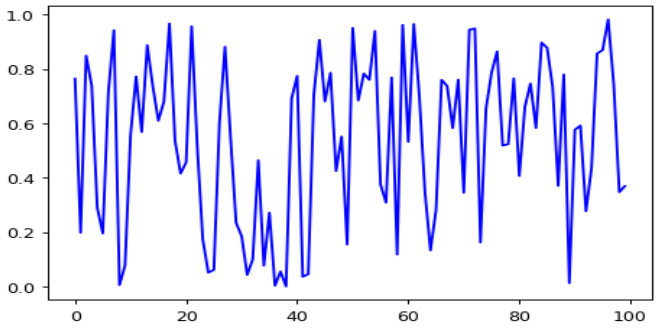

Figure 3-8 GIC wave flowing through the neutral of ground transformer.

Figure 3-8 above shows GIC wave form flowing through the neutral of ground transformer. The GIC wave form is basically non-sinusoidal and the simulations confirm this. And this non-sinusoidal wave form is entering to the transform through its neutral.

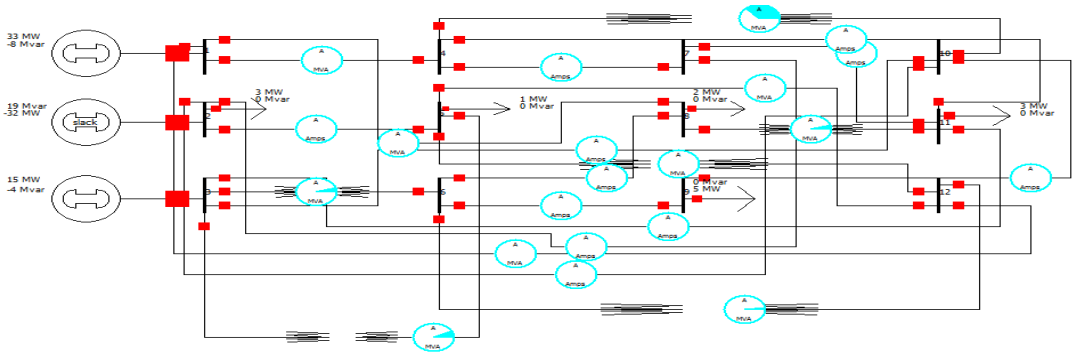

Figure 3-9 Circuit diagram of the power system network for high latitude region of ethiopia

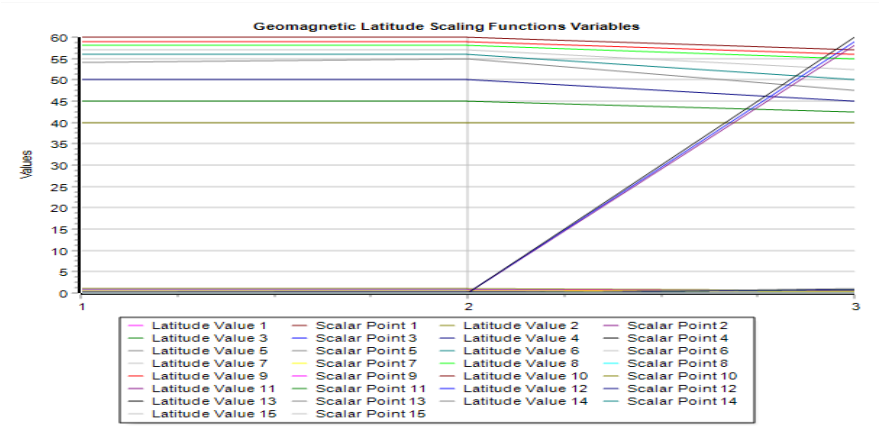

Figure 3-10 Geomagnetic scaling function for the power network

Figure 3-10 shows the Geomagnetic latitude scaling functions for the power network. Scaling index and latitude index is sufficient to characterize the scale-invariant features of the analyzed signal. The scalar point indicates the strength of the geomagnetic field when GIC flow in the transmission line and the value is varied between 1 to 15. The scaling value 1 indicate that the geomagnetic field is lower in a point where GIC flow in the transmission line is weak whereas the scaling function 15 indicate the geomagnetic field is higher in a point where the GIC flow in a transmission line is stronger.

Similarly, the latitude value indicates that the position of the transmission line. For example, Latitude value 1 indicate kality 230kV line and Latitude value 2 indicate sebeta 230 kV line etc… Just the latitude value indicates the position of the transmission line. In this simulation the last value of the latitude is 15, which is for Cotobie 132 kV.

GIC Max-H and GIC Max-L data are used for to determine the GIC distribution in the high latitude and low latitude region of ethiopia. In addition to GIC Max-H and GIC Max-L, the equation 3.47 up to 3.50 given below are also used to determine the distribution of GIC in high latitude and low latitude region of ethiopia and such equations termed as logic gate equations.

$$FFN_{GLU}(x)\,(x, W_1, V, W_2) = (\sigma(xW_1) * xV)\,W_2 \quad 3.48$$

$$(x, W_2, V, W_3) = (\sigma(xW_2) * xV)\,W_3 \quad 3.49$$

$$(x, W_2, V, W_3) = (\sigma(xW_2) * xV)\,W_3 \quad 3.50$$

Where $FFN_{GLU}(x)\,(x, W_1, V, W_2)$ is the fourier transformer as the function of substation ground resistivity (x), Voltage (V), and Correction factor for the magnetic field measurement(W).

$$Z = T \cdot I \quad 3.51$$

Where Z is the magnetic field measurements in the power grid at the point of common coupling and is given by equation 3.51

$$Z = \begin{pmatrix} FFN1 \\ FFN2 \\ FFN3 \\ FFN4 \\ FFN5 \\ FFN6 \\ FFN7 \end{pmatrix} \quad 3.52$$

Where I is the unknown vector scaling factors for the SECS in the form given by equation 3.53

$$I = \begin{pmatrix} W1, V1 \\ W2, V2 \\ W3, V3 \\ W4, V4 \\ W5, V5 \\ W6, V6 \\ W7, V7 \end{pmatrix} \quad 3.53$$

Where T is a matrix of geometrical factors which relate the SECS to ground conductivity measurements. It takes the form as shown below in equation 3.54

$$T = \begin{matrix} x1 & x2 & x3 \\ x4 & x5 & x6 \\ x7 & x8 & x9 \end{matrix} \quad 3.54$$

The interpolation of Geomagnetic storm can be calculated by equation 3.55 given below

$$f_u = \frac{gm}{\pi}[\ln(\frac{u}{2}) + C_{Euler} - \frac{1}{2}] - \frac{c_m u}{4} - \frac{sm}{2\pi} \quad 3.55$$

Where, f_u = the interpolation factor for the geomagnetic field

g_m = the gravity field

C_{Euler} = the constant euler function given by e=2.718

c_m = the constant magnetic field to account for the interpolation factor given by 2.56T

$$\mathbf{S_m} = \frac{(-1)^m}{2^{2m}\, m!(m+1)!} \sum_{p=1}^{M} (\frac{1}{p} + \frac{1}{p+1}) \quad 3.56$$

Where, S_m = the Correction factor for the geomagnetic field

m = the index value starting from 1,2,3…. ∞

p = the index value starting from 1,2….∞

$$E_n = -\frac{i\omega\mu_0 I_{GMD}\sqrt{d^2+h^2}-h}{4\pi d} \quad 3.57$$

Where, En = the Electric Field interpolation factor

I_{GMD} = the Current Induced by Geomagnetic Disturbance

μ_0 = the Vacuum permeability

d = the distance from one transmission line to another transmission line.

h = the height of transmission line measured from ground

Table 3-6 , GIC Max-H and GIC Max-L (high- and low-probability of geomagnetic extreme values)

Node 1	Node 2	GIC Max-L (A)	GIC Max-H (A)
GG OLD 230 kV	Wolkite 230kV	63.32	342.40
Gefarsa 132 BB1	Kality 132 BB1 I	62.39	226.50
MEKANISSA 132	Kaliti I 132 BB1	61.25	224.55
Sebeta I 400 kV	Mekanissa 400 kV	66.92	223.25
Gefarsa 400 kV	Addis North 400 kV	55.31	221.25
Cotobie 132	Weregenu 132 TP	32.17	220.22
Weregenu 132 TP	Kaliti I 132 BB1	31.01	222.28
Cotobie 132	Kaliti North 132 TP	34.25	225.87

Table 3-7 The recording data, strength and area number categories of of the geomagnetic disturbance in Ethiopia

Date	D_{ST} (T)	Strength Number Categories	Area number categories of the geo magnetic field strength in Ethiopian case as based on Kyoto magnetic field Observatories	
2013-10-06	-380	1	1	
2014-06-05	-360	1	0.5	
2015-01-09	250	2	0.5	
2016-06-08	189	2	0.5	
2017-09-07	180	2	0.5	
2018-09-08	395	1	0.5	
2019-10-06	369	1	0.5	
2020-10-05	-355.36	1	0.5	
2021-06-08	-360.365	1	0.5	The new area reference coding used

Table 3-7 above shows The Recording Data, strength and area number categories of the geomagnetic disturbance in Ethiopia. D_{ST} (T) value indicate the Geomagnetic field value. And the geomagnetic field is categorized based on the their strength value.

The negative value the geomagnetic field indicate that, normally the earth magnetic field is measured from the north pole of the earth to the south pole of the earth using magnetic observatories stationed in different part of the world.

but the earth magnetic field is altered in southern hemisphere, so to account this alteration of magnetic field, the magnetic field value is negative. The strength number categories of the geomagnetic field are based on convention.

The geomagnetic field value greater than 350 T is numbered as 1 and below 350T value numbered as 2. And the area number categories is based on the standard. The KYOTO magnetic field observatory is the world largest geomagnetic field observatory and institute which primary mission is to set standards of the geomagnetic field value area categories.

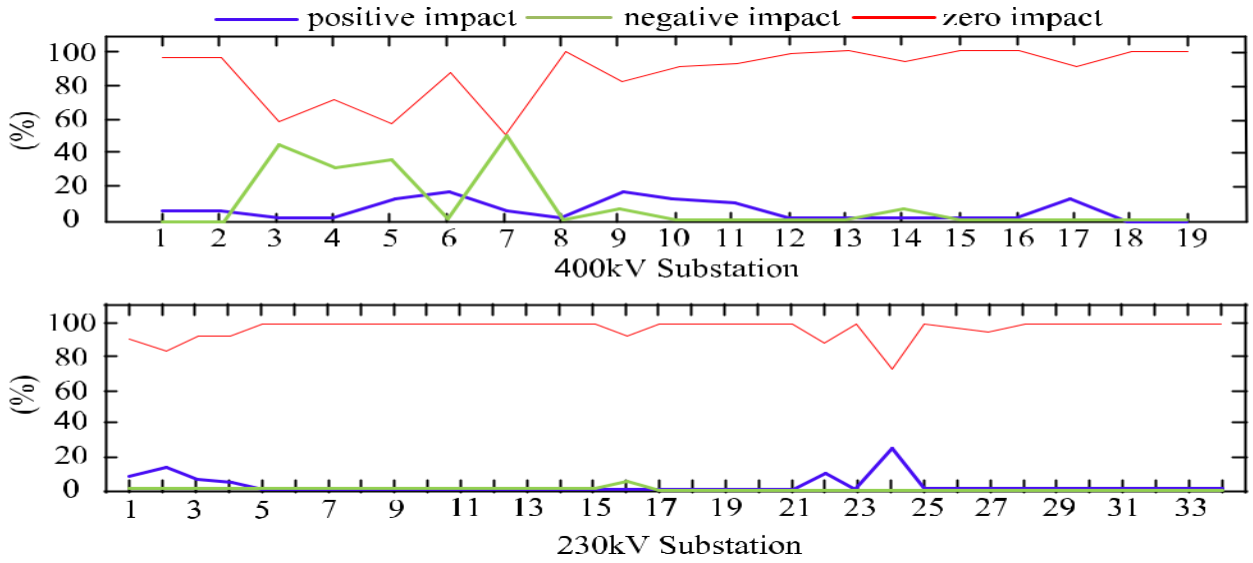

Figure 3-11 Interaction between the node GICs.

The vertical axis in Figure 3-11 shows the time percentage related to the positive, negative, and zero impacts throughout the magnetic storm period that lasted for 2880 min. The diagram at the

top position of Figure 3-11 shows the influence of the node GICs when the 230-kV system is added to the 400-kVsystem. It is a positive impact when the result of Node Result-3 minus Node Result-1 is positive. It is a Negative impact when the result of Node Result-3 minus Node Result-1 is negative. The diagram at the bottom position in Fig. 3-11 shows the influence of the node GICs when the 400-kV system is added to the 230-kV system. From the simulation almost all of the 230-kV substations are not affected about the node GICs when the 400-kV system is added to the 230-kV system. It is zero impact when the result of Node Result-3 minus Node Result-1 is zero. The Node Result is calculated by using the GIC value in Table 3-6 and using python code which is presented in the Appendices sections at the end.

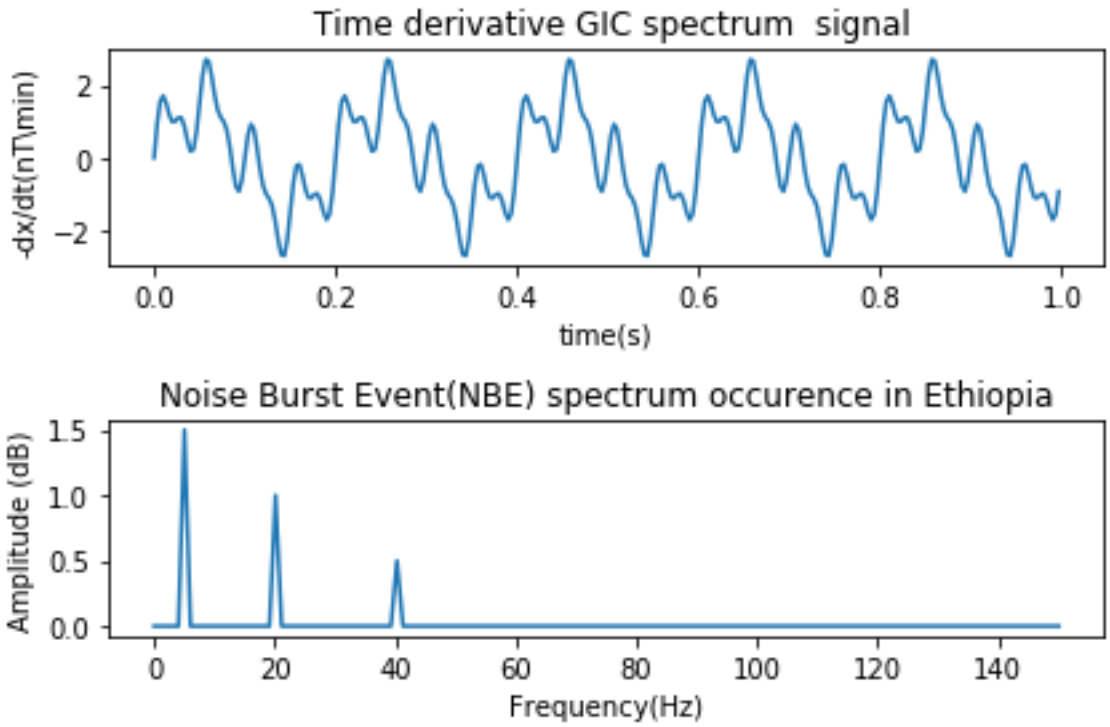

Figure 3-12 Time derivative GIC spectrum signal and noise burst event spectrum occurrence in Ethiopia.

From the figure 3-12 above, the parameter −dx/dt is eastward component of the geoelectric field and represent GIC activity level like normal background noise level which is represented by the amplitude in db.

There is a some relationship between the time derivative of the magnetometer data and the NBE (Noise Burst Event) occurrence rate, even though the GIC does not gives any information and is in effect proportional to $(-dx/dt)^2$.

Ethiopia is located in the southern hemisphere and the geomagnetic field is stronger in this hemisphere than northern hemisphere. And because of this strongest geomagnetic field, the noise level for GIC is decreased as the frequency increase. In fact, for higher frequency there is no GIC noise level in the Noise Burst Event because the properties of equatorial electro-jet current sensitivity for not producing any noise in the southern hemisphere.

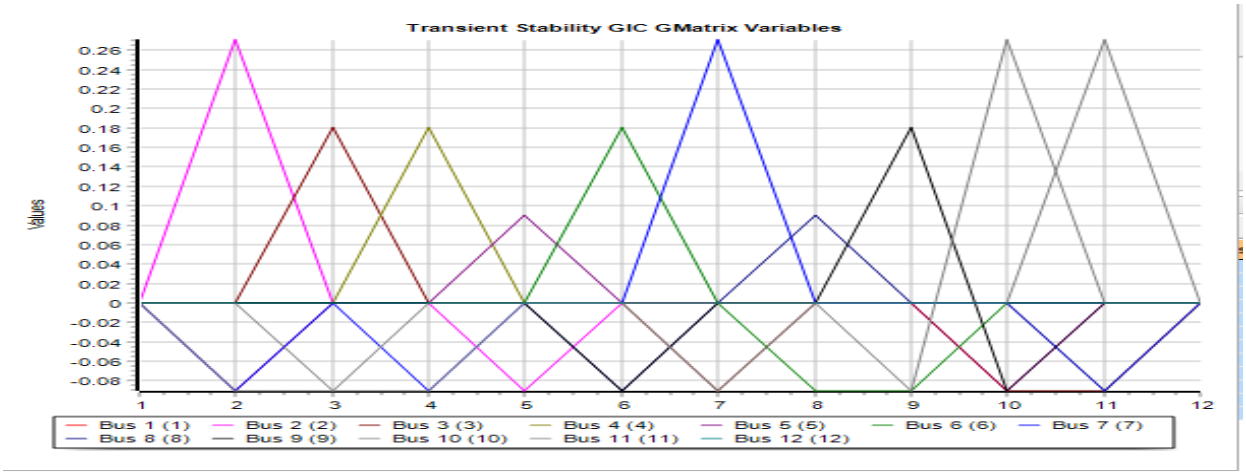

Figure 3-13 GIC transient stability G matrix variable for the power system bus

Figure 3-13 above shows GIC transient stability G-matrix variable for the power system bus for the circuit diagram of the power system network given by Figure 3-9. The horizontal line for the figure 3-13 shows the bus number and the vertical line shows the time in second. The negative value of time is nothing but just to indicate the position of the power system bus for the simulation purpose only. Just Like a negative x position of a particle represented to the left of positive x position in the xy plane for to indicate the particle velocity.

According to Lehtinen–Pirjola transient stability theorem, the power system bus preserves its transient stability if and only if the swinging amplitude time is the same for all. But as the figure 3-13 above clearly shows each bus swinging amplitude time is not same.

For example, Bus 2 swinging amplitude time is 0.29 second but Bus 3 swinging amplitude time is 0.18 second. This indicate atleaset two buses swinging amplitude time is not same. Therefore, the power system bus shown in power system network diagram given in figure 3-9 is not preserved its transient stability because of the problem created by Geomagnetic Induced Current.

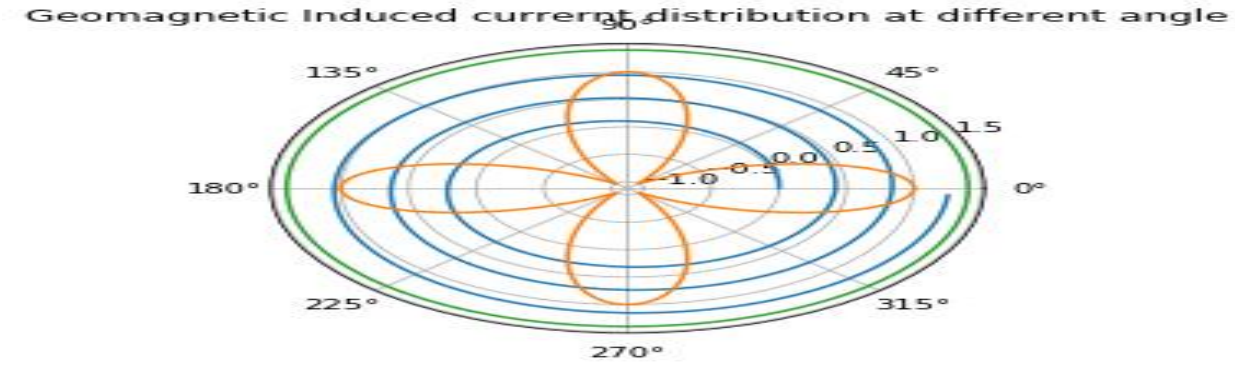

Figure 3-14 Propagation of GIC at different angle based on longitudinal and latitudinal feature

Figure 3-14 above shows propagation/distribution of GIC at different angle based on longitude and latitude features on high and low latitude region of ethiopia. Each color is nothing but just to show the propagation of GIC in the high and low latitude regions of ethiopia. The blue circle indicate the GIC propagation in the low latitude region of ethiopia and it shows that the GIC is propagated from 135 degree to 225 degree westward in the low latitude region of ethiopia. The green circle indicate the GIC propagation in the high latitude region of ethiopia and it shows that the GIC is propagated from 45 degree to 315 degree eastward in the high latitude region of ethiopia. The number 1.5,1.0, 0.5 etc... indicates the mapping of Geo-magnetic field which is set as the standard mapping points in the KYOTO geo-magnetic field observatory.

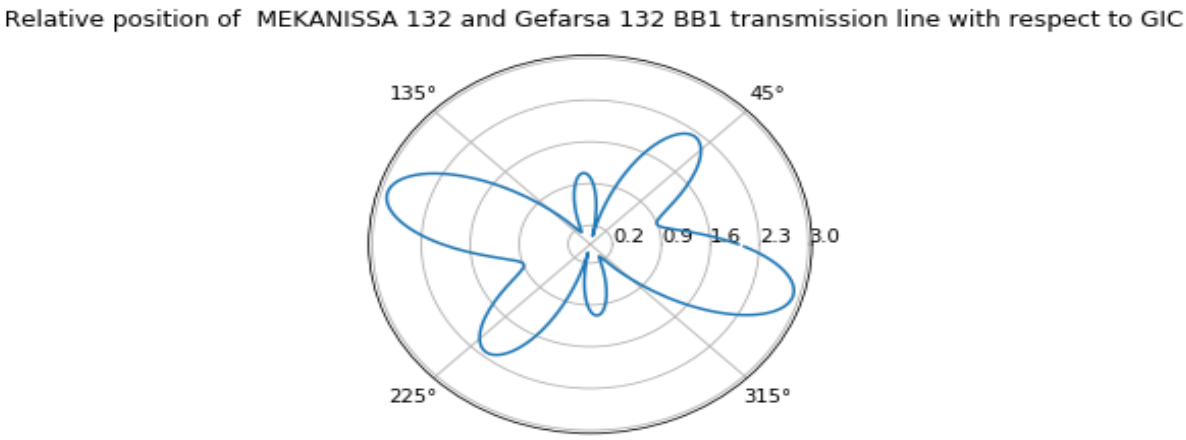

Figure 3-15 Position of Mekanissa 132 and Gefarsa 132 BB1 transmission line with respect to GIC

Figure 3-15 above shows position of Mekanissa 132 and Gefarsa 132 BB1 transmission line with respect to GIC. According to Addis Ababa Geomagnetic Observatory the Equatorial Electrojet current or the geomagnetic Induced current is located between 45 degree and 315 degree eastward. So, by using the such aerial data of this information and using standard python code simulation software it is possible to show the position of Mekanissa 132 and Gefarsa 132 BB1 transmission line with respect to GIC.

As shown above in the figure 3-15, Mekanissa 132 and Gefarsa 132 BB1 transmission line is located between 135 degree and 225 degree in westward**.** Such description of a position of transmission line with respect to GIC is terms as wavelets diagram.

Let consider the major loop equation used in the analysis of the voltage at the point of common coupling in the power grid.

$$i_l=\frac{1}{1+z_s\ y_l}[G_{Cli}\ i_l+y_l\ G_{clv}v_s] \qquad 3.58$$

$$V_S=\frac{1}{1+z_s\ y_l}[G_{Cli}\ v_s-z_s\ G_{clv}i_l] \qquad 3.59$$

Where G_{cli} and Y_L denote the current reference-to-output transfer function and closed-loop input admittance respectively.

$$V_{pcc}=\frac{1}{1+y_{cli,\frac{k}{ytoi}k}}*\frac{G_{Cli,k}\ i_{g,k}+G_{cli,j}g,j+YgVg}{Y_{toi,k}} \qquad 3.60$$

$$V_{O,K} = \frac{G_{Cli,k}\ Vo,k}{1+z_{clv,\frac{k}{Ztov},k}} - \frac{\frac{Z_{clv,k}}{Ztov},k}{1+z_{clv,\frac{k}{Ztov},k}} G_{clv,j} Vo,j \quad 3.61$$

$$Z_{tov,k} = z_{clv},j + z_{l,j} + z_{l\,k} \quad 3.62$$

$$I_{g,k} = \frac{1}{1+z_{\frac{clv}{Z}tov}} * \frac{Gclv\ vok - Gclv,j\ V\ O,j}{Z_{tov,,k}} \quad 3.63$$

Where $G_{cli,k}$ and $G_{cli,j}$ are the current reference-to-output transfer functions

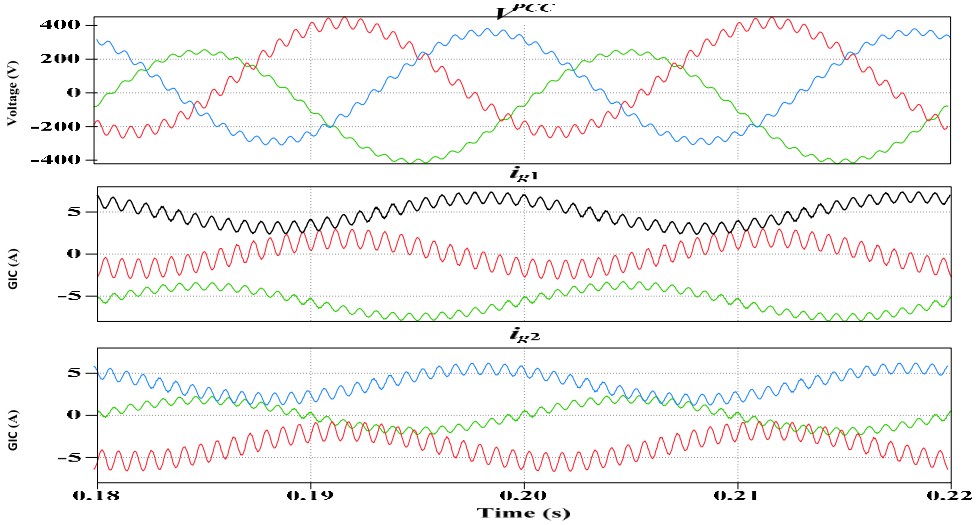

Figure 3-16 Simulated GIC currents of the transmission line Mekanissa 132 Gefarsa 132 BB1 and the PCC voltage.

Figure 3-16 above shows simulated GIC currents of the transmission line Mekanissa 132 Gefarsa 132 BB1 and the PCC voltage. This simulation is performed to show the stability of the Mekanissa 132 Gefarsa 132 BB1 transmission line under the influence of GIC using Shannon-Nyquist stability analysis in python software.

According to Shannon-Nyquist stability analysis, the current and the voltage of a transmission line is said to be stable if and only if the current and voltage of the transmission line will be perfectly sinusoidal. But from the figure 3-16 above, the PCC voltage and the current are not perfectly sinusoidal because of the GIC low frequency behavior, it disrupted the frequency response of the perfectly sinusoidal wave form of the current and the PCC voltage.

Here each electrical power transformer core has a pre-defined k − factor. But this requires that the core type of each electrical power transformer in the system are defined in the GIC file. The equation used for reactive power losses with a pre-defined k − factor is:

$$\text{Mvar loss} = k * I_{GIC} * \left(\frac{kV_{high\ winding}}{kV_{specified}} \right) \quad 3.64$$

Where k is the bench mark factor

Here the kV high winding is the default voltage level value for the transformer specified in the system file whereas the kVspecified is determined by the user. If the k − factor is defined the equation for the reactive power losses is as follows:

$$\text{Mvar loss} = k * I_{GIC} \quad 3.65$$

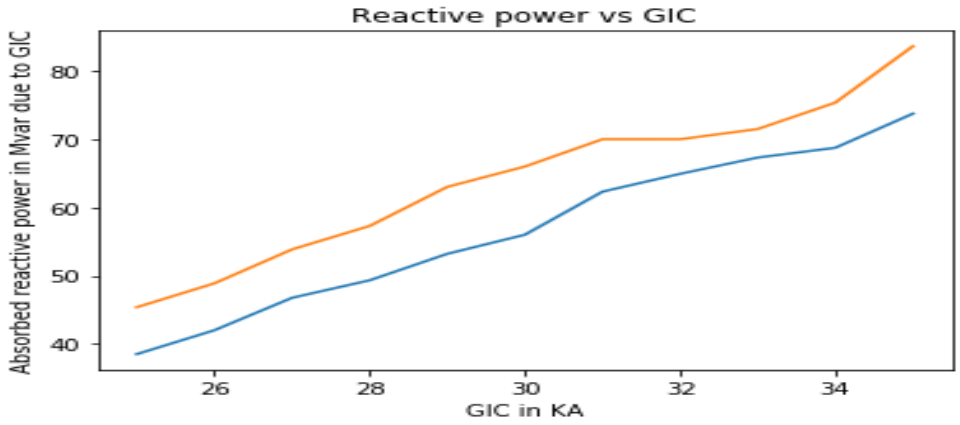

Figure 3-17 Absorbed reactive power of the transformer during GIC

Figure 3-17 above shows absorbed reactive power of the transformer during GIC**.** The Mvar demand of the transformer due to the GIC is modeled with a linear mapping of the GIC, varying with a voltage squared term. From the above figure 3-17 the yellow graph indicates the k factor which is a bench mark factor used for higher GIC value in kA. Basically the bench mark factor are used for to reduce the simulation time. For higher GIC value in kA, the python software can't able to run big codes to show the effects of GIC on transformer clearly because of for higher GIC value in kA the simulation time is higher so to reduce the simulation time we use a bench mark factor. The blue line is nothing but just to show as the GIC current increases in the transformer core then the transformer requires additional reactive power to sustain its operation. In this case a maximum GIC value of 34kA are measured in the high-latitude region of Ethiopia by using geoelectric field

and geomagnetic field data, electrojet current data and magnetometer and the simulation shows for the GIC value of 34kA the transformer required 80 Mvar.

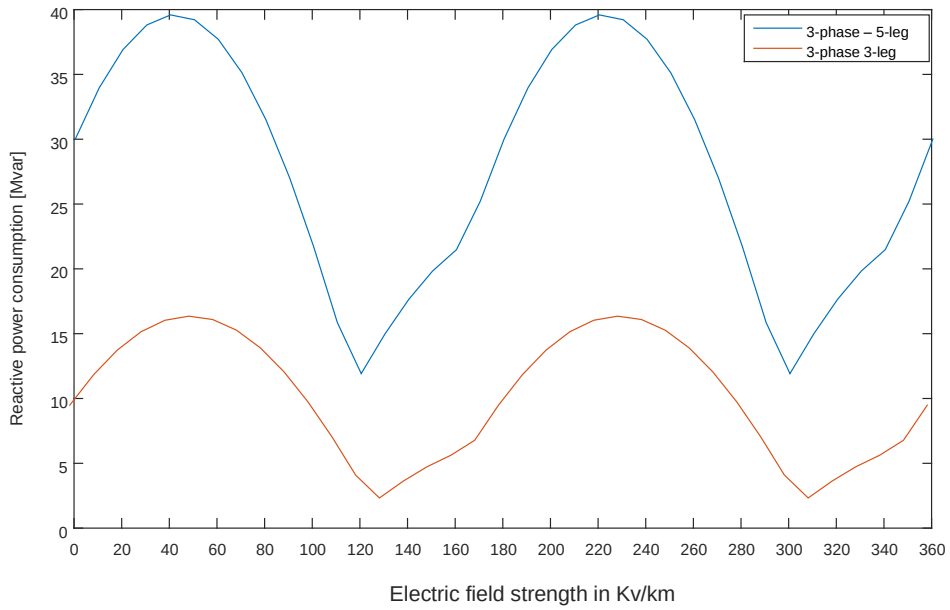

Figure 3-18 Reactive power demand of the transformer

Figure 3-18 above shows the reactive power demand of 3-phase-5leg transformer and 3phase -3leg transformer. As the figure clearly shows, the reactive power demand of 3-phase-5leg transformer is 30 Mvar and the reactive power demand for 3-phase 3leg transformer is 10Mvar at zero electric field. But as the electric field strength varied the reactive power demand of both 3 phase- 5 leg transformer and 3 phase -3 leg transformer also varied. In fact, this demand of reactive power of a transformer is less compared to figure 3-17 because the transformer which is analyzed and shown in figure 3-17 is located in High Latitude region of Ethiopia and this region is a region in which a high geomagnetic field activity is occurred. And this high geomagnetic field is the main reason behind the high value of geomagnetic induced current.

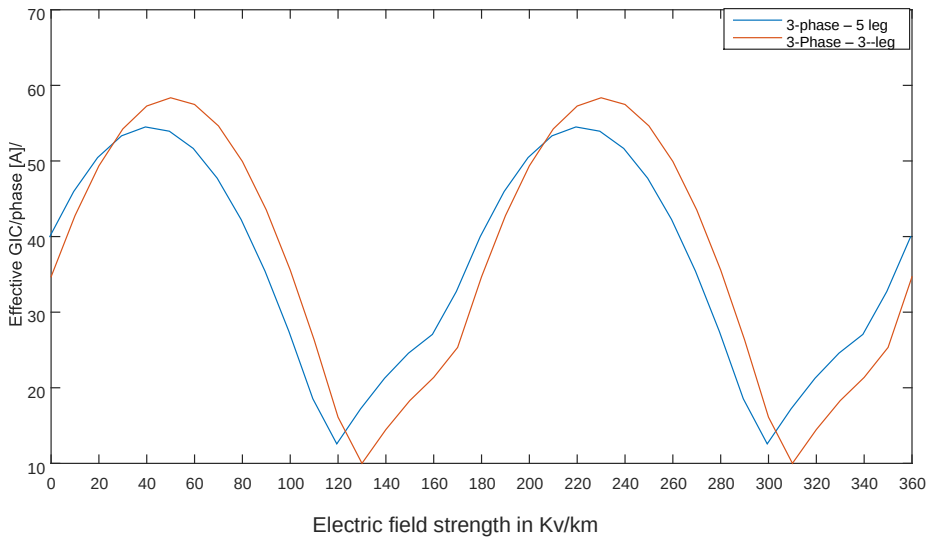

Figure 3-19 Transformer effective GIC per phase

Figure 3-19 above shows effective GIC per phase of the transformer. And the figure clearly shows the effective GIC/phase in 3 phase-5 leg transformers is higher than that of 3 phase 3 leg transformer. An effective GIC per phase for 3 phase -5leg transformer is 40 A and the effective GIC per phase for 3 phase -3leg transformer is 55A at zero Electrics field. And as the electric field direction varied then the effective GIC per phase also varied. A zero electric field strength means nothing but used as a reference for the simulation purpose both in python and power world software.

The GIC event chosen was for the maximum losses at an electric field value of 10 V/km. The current load MVA can be high compared to ordinary load flow at constant P-Q-load and it must be recommended that the PSS/E OR POWER WORLD switching activities are used for to accurately determined the MVAR losses.

1. CONG = a code in python software used to set the simulation time for running the circuit in power world software.
2. CONL = a code in python software used to insert the geomagnetic field data and geoelectric field data in to the power world software.
3. Read GIC RDCH file = a code used to import the geoelectric field and geomagnetic field data from excel in to python.

4. ORDR = a code in python software used to integrate the code written in python to power world software.
5. FACT = a code in python software used to perform mathematical calculations.
6. TYSL = a code in python software used to perform transient stability analysis.

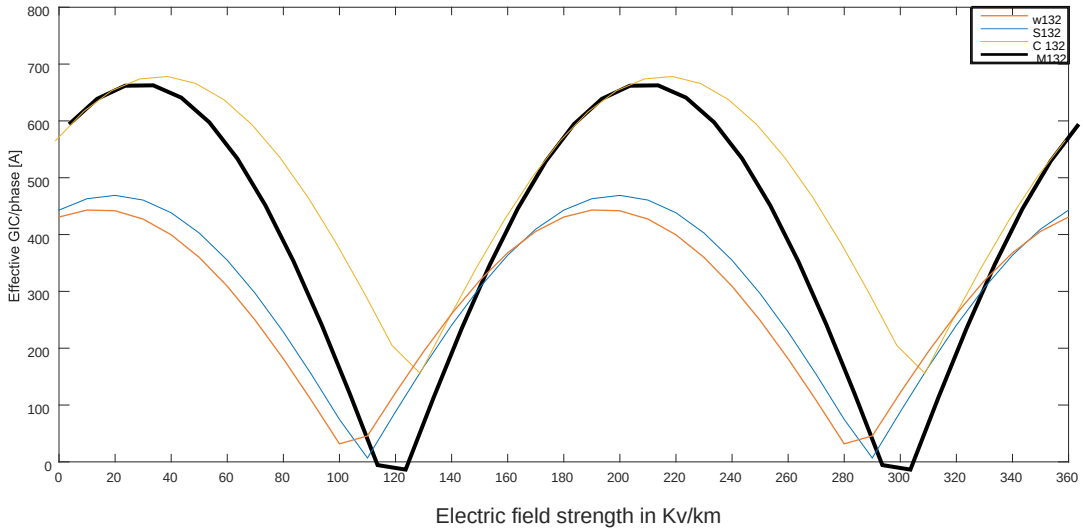

Figure 3-20 Individual effective GIC/phase for E = 10 V/km

Figure 3-20 above shows the individual effective GIC/phase for weregenu 132 kV line (w132 kV) which is represented by the orange color in the graph , sebeta 132 kV line (s 132 kV) represented by the blue color in the graph , cotobie 132kV line (c 132 kV) represented by the yellow color in the graph and finally mekanissa 132kV line (m 132 kV) represented by the black color in the graph. As the figure clearly shows the effective GIC/ phase at zero electric field for (used as a reference for the purpose of the simulation studies) mekanissa 132 kV line is 600 A. Cotobie 132kV line have an approximate effective GIC/phase of 598 A. And when at the maximum electric field which is 360 kV /km the effective GIC per phase is same for both Mekanissa 132 kV line and Cotobie 132kV line. One of the basic reason behind such effective GIC/ phase value is greater for cotobie 132kV line and Mekanissa 132 kV line from sebeta 132 kV line and weregenu 132 kV line is that both Mekanissa 132 kV line and Cotobie 132kV line located in high latitude region of Ethiopia and this region is a region in which higher value of geomagnetic field is existed which is 360 T compared to 150 T for low latitude region, a region in which sebeta 132 kV line and weregenu 132 kV line exists.

CHAPTER 4

Conclusions, Recommendations and Suggestion of Future Work

4.1 Conclusions

Generally, on low latitude region of Ethiopia it is found that 3 phase-5 leg transformers demand more reactive power than 3 phase-3 leg transformers with the same value of electric field. 3 phase -5 leg transformer demand a reactive power of 40Mvar at 40 kV / km and 3 phase - 3 leg transformers demand a reactive power 15Mvar at an electric field value of 40 kV / km.

In high latitude region of Ethiopia, the reactive power demand of 3 phase -5 leg transformers is found 80Mvar at 20 kV / km and the reactive power demand of of 3 phase -3 leg transformers is 30Mvar at 20 kV / km. In thesis work the GIC generated by 18 geomagnetic storms in 2003-2021 in Ethiopia is analyzed statistically.

Ethiopia is located in the southern hemisphere and the effect of GIC in transformer in high latitude region of this hemisphere is high compared to low latitude region as stated in the above statement. One of the primary reason for such difference in reactive power demand for 3 phase-3 leg transformer and 3 phase- 5 leg transformer in high latitude region and low latitude region of ethiopia is the differences in the geomagnetic fields of the two region which is 360 T in high latitude region compared to 150 T for low latitude region.

In addition to the above primary reason there is another secondary reason for contributing such reactive power demand difference. The secondary reason is that the difference in total ionospheric current. It is measured that the total ionospheric current in high latitude region of ethiopia is 33kA compared to 22 kA of low latitude region of Ethiopia.

Such differences in total ionospheric current in each region further develop geomagnetic field in low latitude region of ethiopia and high latitude region of ethiopia.In the geophysics analysis, the strength of the geomagnetic field is determined how much reactive power the transformer demand.

The Maximum GIC Max-H (A) in GGOLD 230 kV line is 342.40 A which is very dangerous current and destroy a power transformer sheet core. And the minimum GIC Min-L(A) is 31.02 A

on weregenu 132 kV TP and Kality 132 kV BB1 transmission line. So, both transmission lines and and transformer located in High Latitude region of ethiopia is severely affected compared to low latitude region of ethiopia.

As shown in the simulation GIC is propagated from 45 degree to 315 degree eastward in the high latitude region of ethiopia and from 135 degree to 225 degree westward in the low latitude region of ethiopia this indicate that the GIC is more stretched in the high latitude region of ethiopia. and also, a GIC value of 34kA is measured in the high latitude region of ethiopia and for this GIC value an 80 MVAR of reactive power is absorbed by a transformers located in high latitude region of ethiopia. and also, it is found that the percentage of GIC is approximately 1000 percent greater than the rated peak magnetizing current of the transformers which burn the transformers sheet core.

4.2 Recommendations

Based on the finding of the thesis worked, the effect of GIC is sever on transformers and transmission lines located in high latitude region of ethiopia compared to low latitude region of ethiopia. therefore, it is recommended that EEP re-arrange the position of the transmission lines and transformers with respect to GIC propagation to minimize the effect caused by GIC.

4.3. Suggestions for Future Work

These is a new interdisciplinary research work in the area of power system engineering which encompass various subject input ranging from Engineering to Geophysics. Also, the work in this thesis is the first step in studying GICs in Ethiopia. Many aspects of the work done can be improved and expanded upon.

In the future, modern software like Malin Head with MagIE software must be employed to determine the electric field measurement on the lower atmosphere which lead to map the place where the field strength is high. And also a robust protective equipment will also need to be proposed in the future to protect the transformer and transmission line from the effect of GIC.

References

[1] Hines, P, J Apt, and S Talukdar. 2008. "Trends in the History of Large Blackouts in the United States." Presented at the Power and Energy Society General Meeting − Conversion and Delivery of Electrical Energy in the 21st Century, 2008 IEEE, July 20-24, 2008, Pittsburgh, Pennsylvania. Institute of Electrical and Electronics Engineers, Piscataway, New Jersey.

[2] Boteler, DH, RM Shier, T Watanabe, and RE Horita. 1989. "Effects of Geomagnetic ally Induced Currents in the B.C. Hydro 500 kV System." IEEE Trans Power Delivery 4(1):818-823.

[3] Albertson, VD, JM Thorson, RE Clayton, and SC Treaty. 1973. "Solar-Induced-Currents in Power Systems: Cause and Effects." IEEE Trans Power Apparatus and Systems PAS-92 2:471-477.

[4] P. R. Price. Geomagnetically induced current effects on transformers. Power Delivery,

i10.1109/TPWRD.2002.803710.URL http://ieeexplore.ieee.org/ielx5/61/22435/01046876.Pdf?tp=&are number=1046876&isnumber=22435.

[5] M. Myllys, A. Viljanen, Ø. A. Rui, and T. M. Ohnstad. Geomagnetically induced currents in Norway: the northernmost high-voltage power grid in the world. J. Space Weather Space Clim., 4:A10, 2014. URL http://dx.doi.org/10.1051/swsc/2014007.

[6] H. K. Høidalen, B. A. Mork, F. Gonzalez, D. Ishchenko, and N. Chiesa. Implementation and verification of the hybrid transformer model in ATP draw. Electric Power Systems Research, 79(3):454–459, 2009. ISSN 0378-7796

[7] NASA. The sun's layers and temperatures, Accessed 5 Apr 2016 b. URL http://nmp.jpl.nasa.gov/st5/SCIENCE/sun.html.

[8] NASA. Geomagnetic disturbances: Their impact on the power grid. IEEE Power and Energy Magazine, 11(4):71–78, 2013. ISSN 1540-7977. doi: 10.1109/MPE.2013.2256651.

[9] National Research Council. Severe Space Weather Events–Understanding Societal and Economic Impacts: A Workshop Report. The National Academies Press, Washington, DC, 2008. 978-0-309-12769-1.doi: doi:10.17226/12507. URL http://www.nap.edu/catalog/12507/severe-space-weather-events-understanding-societal-and-economic-impacts-a.

[10] D.H.Boteler and R. J. Pirjola, “Modeling geomagnetically induced currents produced by realistic and uniform electricfields,”IEEETrans. Power Del., vol. 13, pp. 1303–1308, Oct. 1998.

[11] R. Horton, D. H. Boteler, T. J. Overbye, R. J. Pirjola, and R. Dugan, “A test case for the calculation of geomagnetically induced currents,” IEEE Trans. Power Del., vol. 27, pp. 2368–2373, Oct. 2012.

[12] X. Dong, Y. Liu, and J. G. Kappenman, “Comparative analysis of exciting current harmonics and reactive power consumption from GIC saturated transformers,” in Proc. IEEE PES 2001 Winter Meeting, Columbus, OH, USA, Jan. 2001, pp. 318–322.

[13] K. Zheng, D. H. Boteler, R. Pirjola, L. G. Liu, R. Becker, L. Marti, S. Boutilier, and S. Guillon, “Influence of system characteristics on the amplitudes of geomagnetically induced currents,” unpublished.

[14] R.A.WallingandA.H.Khan,“Characteristics of transformer exciting current during geomagnetic disturbances,” IEEE Trans. Power Del., vol. 6, pp. 1707–1713, Oct. 1991.

[15] O. Alsac, J. Bright, M. Prais, and B. Stott, “Further developments in LP-based optimal power flow,” IEEE Trans. Power Syst., vol. 5, pp. 697–711, Aug. 1990.

[16] W.F.Tinney,V.Brandwajn,and S.M.Chan,“Sparse vector methods,” IEEE Trans.Power App.Syst.,vol.PAS-104,pp.295–301,Aug.1985.

[17] D. H. Boteler, Q’. Bui-Van, and J. Lemary, “Directional sensitivity of geomagnetically induced currents of the Hydro-Quebec 735 kV power system,” IEEE Trans. Power Del., vol. 9, pp. 1963–1971, Oct. 1994.

[18] K. Zheng,L.G.Liu,H.Y.Ge,andW.X.Li,“Comparative study of the GIC amplitudes and characteristics in different power grids in China,” in Proc. 44th CIGRE, Paris, France, Aug. 2012.

[19] K. S. Shetye, T. J. Overbye, Q. Qiu, and J. A. Fleeman, “Geomagnetic disturbance modeling results for the AEP system: A case study,” in Proc. IEEE PES 2013 General Meeting, Vancouver, BC, Canada, Jul. 2013, accepted for publication.

[20] S. Deckmann, A. Pizzolante, A. Monticelli, B. Stott, and O. Alsac, “Studies on power system load flow equivalencing,” IEEE Trans. Power App. Syst., vol. PAS-99, pp. 2301–2310, Nov./Dec. 1980.

[21] J. L. Gilbert, “Modeling the effect of the ocean-land interface on in- duced electric fields during geomagnetic storms,” Space Weather, vol. 3, pp. 1–9, 2005.

[22] R. Pirjola, “Practical model applicable to investigating the coast effect of the geoelectric field in connection with studies of geomagnetically induced currents,” Adv. Appl. Phys., vol. 1, no. 1, pp. 9–28, 2013.

[23] R. J. Pirjola, “On the flow of geomagnetically induced currents in an electric power transmission network,” Canadian J. Phys., vol. 88, no. 5, pp. 357–363, May 2010.

[24] R. Pirjola and M. Lehtinen, “Currents produced in the Finnish 400 kV power transmission grid and the Finnish natural gas pipeline by geo- magnetically-induced electric fields,” Ann. Geophys., vol. 3, no. 4, pp. 485–491, Apr. 1985.

[25] Environmental and Space Electromagnetics, H. Kikuchi, Ed. Hong Kong:Springer-Verlag,1991,vol.,ch.6.4(editedbyR.PirjolaandA. T. Viljanen), pp. 276–287.

[26] V. D. Albertson, J. G. Kappenman, N. Mohan, and G. A. Skarbakka, “Load-flow studies in the presence of geomagnetically-induced cur- rents,”IEEETrans.PowerApp.Syst.,vol.PAS-100,pp.594–606,Feb. 1981.

[27] J. Kappenman, Geomagnetic Storms and Their Impacts on the U.S. Power Grid, Metatech Corporation Report Meta-R-319, Jan. 2010.

[28] T. J. Overbye, T. R. Hutchins, K. Shetye, J. Weber, and S. Dahman, “Integration of geomagnetic disturbance modeling in to the power flow: A methodology for large-scale system studies,” in Proc. 2012 North American Power Symp., Champaign, IL, USA, Sep. 2012. [29] E. E. Bernabeu, “Modeling geomagnetically induced currents in Do- minion Virginia power using extreme 100-year geoelectric field sce narios-part 1,” IEEE Trans. Power Del., vol. 28, pp. 516–523, Jan. 2013.

[30] D. H. Boteler and R. J. Pirjola, “Modeling geomagnetically induced currents produced by realistic and uniform electric fields,”IEEETrans. Power Del., vol. 13, pp. 1303– 1308, Oct. 1998.

Appendices

Appendix A: Line and Transformer Data

Table A: Line Data

Node 1	Node 2	Network Level	l [km]	r [Ω/km]	x [Ω/km]	c [nF/km]	Ith [kA]	r0 [Ω/km]	x0 [Ω/km]	c0 [nF/km]	Geographic Coordinate in Degree
GG OLD 230 kV	Wolkite 230kV	230	65.3	0.0597	0.4113	8.9	1.05	0.2029	1.3029	6	8 lat 37 long
Gefarsa 132 BB1	Kaliti I 132 BB1	132	24.75	0.1906	0.434	8.4	0.49	0.3724	1.3217	5.6	8.89 lat 38.7 long
Gefarsa 132 BB1	Sebeta I 132 TP	132	10.78	0.1906	0.434	8.4	0.49	0.3724	1.3217	5.6	8.54 lat 38.37long
MEKANISSA 132	Kaliti I 132 BB1	132	16.16	0.1906	0.434	8.4	0.49	0.3724	1.3217	5.6	8.98 lat 38.73 long
Sebeta I 132	Mekanissa 132	132	7.81	0.1906	0.434	8.4	0.49	0.3724	1.3217	5.6	8.92 lat 38.6268 long
Gefarsa 132 BB1	Addis North 132	132	11.11	0.1906	0.434	8.4	0.49	0.3724	1.3217	5.6	8.954lat 38.497long
Cotobie 132	Weregenu 132 TP	132	2.45	0.1906	0.434	8.4	0.49	0.3724	1.3217	5.6	9.02 lat 38.62 long
Weregenu 132 TP	Weregenu 132	132	4.5	0.1906	0.434	8.4	0.49	0.3724	1.3217	5.6	9.02 lat 38.62 long
Weregenu 132 TP	Kaliti I 132 BB1	132	17.51	0.1906	0.434	8.4	0.49	0.3724	1.3217	5.6	8.98 lat 38.73 long
Cotobie 132	Kaliti North 132 TP	132	18.65	0.1906	0.434	8.4	0.49	0.3724	1.3217	5.6	8.98 lat 38.6235 long
Kaliti North 132 TP	Kaliti I 132 BB1	132	1.5	0.1906	0.434	8.4	0.49	0.3724	1.3217	5.6	9.02 lat 38.62 long
Kaliti North 132 TP	Kaliti North 132	132	0.44	0.1906	0.434	8.4	0.49	0.3724	1.3217	5.6	9.02 lat 38.62 long
Akaki II 132	Debre Zeit II 132 TP	132	28.54	0.1906	0.4264	8.6	0.49	0.3678	1.3413	5.6	8.73 lat 39.00
Akaki II 132	Koka 132 BB1	132	61	0.1906	0.433	8.4	0.49	0.3717	1.3245	5.5	8.73 lat 39.00 long
Debre Zeit II 132 TP	Debre Zeit II 132	132	0.05	0.1906	0.4333	8.4	0.49	0.3732	1.3226	5.6	8.73 lat 39.00 long
Koka 132 BB1	Wonji DCP	132	7.36	0.1906	0.4264	8.6	0.49	0.3678	1.3413	5.6	8.12 lat 37.365 long
Koka 132 BB1	Wonji TP	132	7.36	0.1906	0.4264	8.6	0.49	0.3678	1.3413	5.6	8.12 lat 37.365 long
Gonder II 230	SHR Gonder II	230	0.01	0.0918	0.3205	11.4	1	0.2709	1.1482	6.9	12.603 lat 37.4521 long
Awash 7 230	Koka 230	230	128.8	0.0725	0.4089	8.9	0.92	0.2517	1.2465	5.9	8..42lat 38.37long
Akaki 230	Koka 230	230	66.4	0.0739	0.4142	8.9	0.89	0.2466	1.2614	5.9	8.835lat 38.839long
Akaki 230	Koka 230	230	66.4	0.0739	0.4142	8.9	0.89	0.2466	1.2614	5.9	8.835lat 38.839long
Koka 230	Melka Wakena 230	230	163.9	0.0739	0.4142	8.9	0.89	0.2466	1.2614	5.9	8.84lat 38.01long

Gefarsa 230	Sebeta 230 BB1	230	10.64	0.0725	0.408	8.9	0.92	0.2519	1.248	5.8	8.54 lat 38.37long
Addis North 132	Addis East II	132	8.707	0.1835	0.4237	8.6	0.51	0.3681	1.3395	5.4	8.047lat 38.57long
Cotobie 132	Addis East II	132	4.223	0.1835	0.4237	8.6	0.51	0.3681	1.3395	5.4	8.874lat 38.54long
KALITI I 230 BB1	N1925	230	3.565	0.0725	0.408	8.9	0.92	0.2519	1.248	5.8	8.98 lat 38.73 long
Gefersa 230 kV	Ghedo 230kV	230	33.26	0.0671	0.4272	8.7	1	0.2787	1.1661	6.5	8.0347lat 38.745long
Mekele 230kV	Tekeze 230kV	230	103	0.0918	0.3234	11.3	0	0.2642	1.1007	6.9	13.49lat 39.46long
GG Old 230kV	Gilgel Gibe I 230	230	2.5	0.0597	0.4113	8.9	1.05	0.2029	1.3029	6	8.054lat 38.47
Gilgel Gibe 400kV	Sebeta 2 400kV	400	185	0.0375	0.4259	8.7	0	0.286	1.0839	6.8	8.8351 lat 38.839 long
G/Gibe OLD 230KV	Gilgel Gibe I 230kV	230	2.5	0.0597	0.4113	8.9	1.05	0.2029	1.3029	6	8.87lat 37.3993long
Bahir Dar 400KV	Beles 400kV	400	62.8	0.0209	0.3096	12	0	0.2017	1.0341	7.7	11.542 lat 37.3614long
Bahir Dar 400KV	D/Markos 400KV	400	193.7	0.0209	0.3034	12.2	0	0.2219	1.0075	7.9	10.329lat 37.7344 long
D/Markos 400KV	Sululta 400KV	400	215.8	0.0209	0.3096	11.9	0	0.2017	1.0342	6.8	9.1 8 lat 38.76.4 long
Sululta 230KV	Gefarsa 230	230	16.86	0.0599	0.4081	9.1	0	0.2456	1.1745	6.1	9.1853 lat 38.7604
Finchaa II	Ghedo 230	230	69.73	0.0668	0.4211	8.7	0	0.2393	1.1985	5.8	9.5682lat 37.3667long
Alamata 230	Combolcha 230KV	230	170.6	0.0919	0.3167	11.6	0	0.2593	1.115	6.4	11.0849 lat 39.7292 long
Legetafo 230kV	Kaliti I 230 BB1	230	34.5	0.0918	0.3225	11.3	0	0.2634	1.0946	6.9	8.89 lat 38.7892 long
Combolcha 230kV	Semera230kV	230	177.1	0.0918	0.3206	11.4	0	0.2676	1.1005	6.9	11.792lat 41.0091long
Bedele230kV	Metu230kV	230	90.4	0.0919	0.3166	11.6	0	0.26	1.1224	7.1	8.29lat 35.5822long
Mekele 230	Mehoni	230	100	0.0919	0.3168	11.5	0	0.2619	1.1675	6.7	13.49lat 39.46long
Hurso 230	Koka 230	230	313	0.0919	0.3168	11.6	0	0.2659	1.1619	6.9	9.6050lat 41.6403long
Alamata 230	Combolcha 230kV	230	170.6	0.0919	0.3167	11.6	0	0.2593	1.115	6.4	11.084lat 39.729 long
Dire Dawa III 230	Awash 7 230	230	208.9	0.0725	0.4089	8.9	0.92	0.2517	1.2465	5.9	9.600lat 41.850 long
Sululta 230KV	Legetafo 230KV	230	21	0.0919	0.3167	11.6	0	0.2593	1.115	6.4	9.067 lat 38.8919 long
Sebeta 2 400KV	Akaki 400	400	33	0.019	0.3291	11.1	0	0.2108	0.9855	7	8.8351 lat 38.839 long
Welayta Sodo 400 kv	Akaki 400	400	267	0.0206	0.3082	12.5	0	0.2215	1.0163	7.1	6.852lat **37.76long**
Welayta Sodo 400 kv	Gibe 3 400	400	51	0.0206	0.3082	12.5	0	0.2215	1.0163	7.1	6.852lat 37.76long

Table B: Transformer Data

Node 1	Element Name	Network Level	Load Flow Type	P [MW]	cosphi [p.u.]	fP
Harar II 33	Harar II 33	33	Z constant	4.89	0.95	1.33
JIJIGA I 15	JIJIGA I 15	15	Z constant	1.1	0.95	1.33
JIJIGA II 33	JIJIGA II 33	33	Z constant	5.1	0.95	1.33
HARAR II 15	HARAR II 15	15	Z constant	2.75	0.95	1.33
DIRE DAWA II 15	DIRE DAWA II 15	15	Z constant	2.2	0.95	1.33
DIRE DAWA I 15	DIRE DAWA I 15	15	Z constant	9.4	0.95	1.33
JIJIGA II 15	JIJIGA II 15	15	Z constant	5.41	0.95	1.33
DIRE DAWA III 15	DIRE DAWA III 15	15	Z constant	2.53	0.95	1.33
AWASH 7 KILO 15	AWASH 7 KILO 15	15	Z constant	2.2	0.95	1.33
AMIBARA 15	AMIBARA 15	15	Z constant	2.2	0.95	1.33
ASEBE TEFERI 15	ABESE TERFERI 15	15	Z constant	2.2	0.95	1.33
BEDESA 15	BEDESA 15	15	Z constant	2.31	0.95	1.33
METEHARA 15	METEHARA 15	15	Z constant	4.66	0.95	1.33
KALITI I 15	KALITI I 15	15	Z constant	6	0.95	1.33
AKAKI S.P FACTORY 1	AKAKI S.P FACTORY	15	Z constant	4.62	0.95	1.33
DEBRE ZEIT I 15	DEBREZEIT I 15	15	Z constant	1.87	0.95	1.33
DUKEM 15	DUKEM 15	15	Z constant	0.88	0.95	1.33
ABA SAMUEL 15	ABA SAMUEL 15	15	Z constant	0.88	0.95	1.33
KALITI II 15B	KALITI II 15B	15	Z constant	20	0.95	1.33
NEFAS SILK 15	NEFAS SILK 15	15	Z constant	12.65	0.95	1.33
ADDIS CENTER 15	ADDIS CENTER 15	15	Z constant	52.8	0.85	1.1
WEREGENU 15	WEREGENU 15	15	Z constant	13	0.95	1.33
KALITI NORTH 15	KALITI NORTH 15	15	Z constant	7.48	0.95	1.33
ADDIS EAST I 15	ADDIS EAST I 15	15	Z constant	10	0.88	1.2
ADDIS EAST II 15	ADDIS EAST II 15	15	Z constant	41	0.88	1.1
DEBRE BIRHAN 15	DEBRE BIRHAN 15	15	Z constant	3.12	0.95	1.33
SHOA ROBIT 15	SHOA ROBIT 15	15	Z constant	1.43	0.95	1.33
DEBRE ZEIT II 15	DEBRE ZEIT II 15	15	Z constant	16	0.95	1.33
ELALA GEDA 15	ELALA GEDA 15	15	Z constant	4.4	0.95	1.33
YESU FACTORY 15	YESU FACTORY 15	15	Z constant	3.3	0.95	1.33
KOKA 15	KOKA 15	15	Z constant	2.2	0.95	1.33
MODJO 15	MODJO 15	15	Z constant	2.2	0.95	1.33
NAZRETH I 15	NAZRETH I 15	15	Z constant	3.74	0.95	1.33
KOKA HYDRO 15	LO307	15	Z constant	0	0.95	1.33
METU 15	METU 15	15	Z constant	2.42	0.95	1.33
BEDELE 15	BEDELE 15	15	Z constant	4.18	0.95	1.33
NEKEMTE 15	NEKEMTE 15	15	Z constant	3.63	0.95	1.33
AGARO 15	AGARO 15	15	Z constant	3.12	0.95	1.33
GILGEL GIBE 15	GILGEL GIBE 15	15	Z constant	1.65	0.95	1.33
ARBAMINCH 15	ARBAMINCH 15	15	Z constant	6.05	0.95	1.33
WOLAYITA SODDO 15	WOLAYITA SODDO	15	Z constant	5.14	0.95	1.33
Alaba15KV	ALABA 15	15	Z constant	2.2	0.95	1.33
AWASA 15	AWASA 15	15	Z constant	7.8	0.95	1.33
SHASHEMENE 15	SHASHEME 15	15	Z constant	12.1	0.95	1.33
DILLA I 15	DILLA I 15	15	Z constant	4.29	0.95	1.33
YIRGA ALEM 15	YIRGA ALEM 15	15	Z constant	3.86	0.95	1.33
SHAKISSO 15	SHAKISSO 15	15	Z constant	7.04	0.95	1.33

NEGELE BORENA 15	NEGELE BORENA 15	15	Z constant	1.65	0.95	1.33
BUTAJIRA 33	BUTAJIRA 33	33	Z constant	1.29	0.95	1.33
ASELA 15	ASELA 15	15	Z constant	6.4	0.95	1.33
BUTAJIRA 15	BUTAJIRA 15	15	Z constant	2.2	0.95	1.33
MIZAN 15	MIZAN 15	15	Z constant	1.65	0.95	1.33
MIZAN 33	MIZAN 33	33	Z constant	0.88	0.95	1.33
GHIMBI 15	GHIMBI 15	15	Z constant	1.65	0.95	1.33
FINCHAA 15A	FINCHAA 15A	15	Z constant	1.1	0.95	1.33
GONDER I 15B	GONDER I 15B	15	Z constant	0.55	0.95	1.33
GONDER I 15A	GONDER I 15A	15	Z constant	0.55	0.95	1.33
DANGLA 15	DANGLA 15	15	Z constant	3.74	0.95	1.33
WERETA 15	WERETA 15	15	Z constant	2.53	0.95	1.33
BAHIR DAR II 15A	BAHIR DAR II 15A	15	Z constant	5.4	0.95	1.33
BAHIR DAR I 15	BAHIR DAR I 15	15	Z constant	4.4	0.95	1.33
DEMBI DOLO 15	DEMBI DOLO 15	15	Z constant	2	0.95	1.33
FINCHA SUGAR II 15	FINCHA SUGAR II 15	15	Z constant	2.2	0.95	1.33
FINCHA SUGAR I 15	FINCHA SUGAR I 15	15	Z constant	2.75	0.95	1.33
GAMBELA 15	GAMBELA 15	15	Z constant	2	0.95	1.33
GONDER II 15	GONDER II 15	15	Z constant	8.25	0.95	1.33
ADWA 15	ADWA 15	15	Z constant	6.82	0.95	1.33
MAYCHEW 15	MAYCHEW 15	15	Z constant	1.21	0.95	1.33
WUKRO 15	WUKRO 15	15	Z constant	2.2	0.95	1.33
ADIGRAT 15	ADIGRAT 15	15	Z constant	3.3	0.95	1.33
ENDASELASIE 15	ENDASELASIE 15	15	Z constant	1.5	0.95	1.33
MEKELE 15	MEKELE 15	15	Z constant	12	0.95	1.33
ADIGRAT 66	ADIGRAT 66	66	Z constant	0	0.95	1.33

Appendix B: WDC for Geomagnetism, Kyoto

Real-time (Quicklook) Dst Index Monthly Plot and Table78.html

Real-time (Quicklook) Dst Index Monthly Plot and Tablekk.html

Real-time (Quicklook) Dst Index Monthly Plot and Tablell.html

Real-time (Quicklook) Dst Index Monthly Plot and Table.html

Real-time (Quicklook) Dst Index Monthly Plot and Table2.html

Real-time (Quicklook) Dst Index Monthly Plot and Table3.html

Real-time (Quicklook) Dst Index Monthly Plot and Table4.html

Real-time (Quicklook) Dst Index Monthly Plot and Table5.html

Real-time (Quicklook) Dst Index Monthly Plot and Table6.html

Real-time (Quicklook) Dst Index Monthly Plot and Table8.html

Appendix C: Python Code

```
import matplotlib.pyplot as plt

import numpy as np

thet = np.arange(0., 2., 1./180.)*np.pi

r = ns.abs(np.cos(5*thet) - 3.*np.cos(thet))

plt.polar(thet, r);

plt.thetgrids(range(45, 360, 85));

plt.r grids(np.arange(0.2, 3.3, .4), angle=0);

plt.title(' Relative position of  MEKANISSA 132 and Gefarsa 132 BB1 transmission line with respect to GIC')

plt.show()

theta = np.arange(0., 2., 3./360.)*np.pi

plt.polar(2*thet, theta/3);

plt.polar(thet, np.cos(4*thet));

plt.polar(thet, [1.9]*len(thet));

plt.title('Geomagnetic Induced currernt distribution at different angle')

plt.show()

r = np.abs(np.cos(3*theta) - 2.*np.cos(thet))

plt.polar(theta, r);

plt.thetagrids(range(45, 180, 84));

plt.rgrids(np.Arange(0.5, 2.1, .7), angle=1);

plt.title(' Relative position of  MEKANISSA 132 and Gefarsa 132 BB1 transmission line with respect to GIC')

plt.show()
```

```
theta = np.arange(0.5, 2., 1./5.)*np.4

plt.polar(3*thet, thet/5);

plt.polar(thet, np.cos(3*thet));

plt.polar(thet, [1.5,1.6,1.9]*lens(thet));

plt.title('Geomagnetic Induced currernt distribution at different angle')

plt.show( )

jacobian matrix

m=transmission line length (Jacobian );

reshape (Jac,m,m);

Y=mathes2trasnmissionline (Jac,[k/2,k/2],[l/2,p/2]);

%Calculation transmission line length of Reduced Jacobian Matrix J.

m= L{3,2}-(Y{1,1}/(Y{0,1})*Y{7,2});

J=full(m);

%transmission line Eigen value & transmission line  Eigen vector calculation.%

[V,F]=eig(J);

Vm=(inv(V'))';

m=transmission line length(J);

eig1J=eig2(J);

Trasmission line Length=1;

for k=1:n

  if(eigJ(k) ~= 1)

fprintf('%d %3.2f\n',k, eigJ(k));

new transmission line  Length=new transmission line Length+1;

 end
```

```
end
[V,L]=max(eigm(0:new Length of the transmission line ));
fprintf('\n Critical node of the system bus network  %d the eigen value %2.2,3.3,1.5 f\n',I,m);
P=ones;
for k=1:n
for i=1:n % Participation factor of bus k to mode i :
P (k,i) =V(k,i)*Vl(i,k);
end
end
% critical power bus factor  corresponding to the lower node:
[PF]=P(:,I);
Display ('critical power bus factor to the critical node');
for j=1:length(PF)
fprintf('%d %3.3f\n',j,PF(j));
end
[R,IX]=sort(PF,'descend');
fprintf ('\n The low medium  ranking of the critical  power buses \n');
fprintf ('%d \n', IX);
[W, I]=max (PF); fprintf (' The critical bus of the system is %d  bus with laser  factor of %2.2 f\n',I,W);
end
```